ESTIMATION OF PHYSICO-CHEMICAL PROPERTIES OF COAL SLAGS AND ASHES

K C MILLS
National Physical Laboratory, Teddington, Middx, TW11 OLW, UK.

1. INTRODUCTION.

Slags formed during the gasification of coal usually contain SiO_2, Al_2O_3, iron oxides, CaO, Na_2O and K_2O with minor amounts of various other oxides. A knowledge of the physico-chemical properties of these slags can improve the control of the process eg. the amount of flux required to bring the slag viscosity to a level suitable for tapping can be calculated from viscosity-composition relations. Physical property data for the coal slags can also improve process design by the development of reliable mathematical models of the process eg. thermal properties of the slags are needed for heat balance calculations. There is an appreciable variation in the compositions of slags formed from various coals and even from different batches of the same stock on occasions and these compositional variations can give rise to considerable differences in the physical properties. As the chemical analysis is frequently available on a routine basis it would be particularly desirable to have reliable models for the prediction of physico-chemical properties from their chemical composition. Furthermore such models would have the further advantage that they would eliminate the need for arduous interpolations on pseudo-ternary plots for slags which are really multicomponent and interactive systems.

The properties of slags are dependent not only upon chemical composition, but upon other factors also. The most pronounced deviations from addivity rules based on composition arise in the estimation of those properties which involve ionic transport such as electrical conductivity. However surface tension values estimated from additivity rules are frequently in error as bulk thermodynamic properties do not apply at surfaces. Furthermore, virtually all the physical properties of slags are, to some extent, dependent upon the structure of the slag (viz. the length of silicate chains,degree of crystallinity etc.) thus estimation procedures have to accommodate these structural factors, where possible.

There is only a limited amount of physical property data available for coal slags and consequently it has been necessary to examine a much broader range of silicates including magmatic liquids and those slags encountered in steelmaking, glassmaking and non-ferrous processes. Thus the models cited here should have a much wider range of application than coal gasification.

A critical evaluation of the extant physical property data has shown that virtually every physical property is markedly dependent upon the distribution of iron in the slag between FeO, Fe_2O_3 and free iron. Frequently these distributions are not reported and they can not be easily predicted as they are very dependent upon (i) the partial pressure of oxygen, p_{O_2}[1] (ii) temperature[1] T and (iii) the nature of the other oxides present, eg CaO, Na_2O and K_2O[1][2][3] increase the amount of Fe_2O_3 and SiO_2 increases the amount of FeO present. Even when the iron distributions are cited they are vulnerable to error owing to difficulties in chemical analysis and the possibility of some redistribution of the $Fe/Fe^{2+}/Fe^{3+}$ ratios during the quench. Nevertheless it is strongly recommended that all future physical property determinations on coal slags should be accompanied by chemical analysis for Fe(free), FeO and Fe_2O_3 on the quenched specimen as the surface tension, absorption coefficient, melting range etc. fluctuate dramatically with the iron distribution.

2. MODELS FOR ESTIMATING PHYSICO-CHEMICAL PROPERTIES.

2.1 Melting Range

Empirical rules have been formulated[4-6] for the estimation of melting range on the basis of the basicity of the slag or ash. However the various constants used in the calculations are applicable to very narrow compositional ranges and thus a large number of constants are required to represent the slags formed from different coals.

A more universal approach has been adopted recently by Gaye[7,8] who expressed, the dependency of liquidus temperature, T_{liq}, upon chemical composition as polynomial for each of the phases (or compounds) formed by the slag. The *maximum* calculated value of T_{liq} value for the various phases is the T_{liq} value. Good agreement was obtained between the calculated and experimental values for T_{liq} for the $SiO_2 + Al_2O_3 + MgO + FeO$ and the $SiO_2 + Al_2O_3 + MgO + CaO$ systems. However development of this model to cover the multicomponent coal slags could prove difficult.

A second model due to Gaye[9] would appear to offer more promise; it is based on the Kapoor-Frohberg model for the estimation of activities and assumes that both acidic and basic oxides are made up of symmetrical cells and that these interact to form assymmetrical cells. The activities of the various oxides calculated for quaternary slags with this model are in excellent agreement with those determined experimentally. Values of T_{liq} for a given composition can be derived by determining the temperature at which the solid phase formed has an activity of one. The model has been developed for systems based on seven components, SiO_2, Al_2O_3, CaO, MgO, FeO, Fe_2O_3 and MnO. The model will have to be enlarged to include Na_2O etc. before it can be used for the reliable estimation of T_{liq} of coal slags but it would seem to have considerable promise and has the decided advantage that it also produces activity data for the various component oxides.

2.2 Viscosity (η)

Several models have been reported for the estimation of viscosities (η) of silicate melts to cover the compositional ranges of glasses[10,11] steelmaking slags[12-14], *magmas*[15-18] and coal slags and ashes[19-24]. The temperature (T) dependence of the viscosity is expressed in the form of the Arrhenius relationship (equation 1)) or the Frenkel relationship (equation 2) which is sometimes known as the Weymann equation) where A and B are constants, E is the activation energy and R is the Gas Constant.

$$\eta = A \exp.(E/RT) \qquad 1)$$

$$\eta = AT \exp.(E/RT) \qquad 2)$$

Estimated viscosities have been calculated using these various models and the closest agreement with experimental values was obtained with the models due to Riboud *et al*[13] and Urbain *et al*[17,18]. These estimation procedures use the Frenkel relationship and thus their superiority may be largely due to the use of equation 2). The model due to Schobert which involves petrographic classification of the coal slag has not been checked and this procedure may provide reliable estimates of viscosity for coal slags but could not be applied to slags covering a wide range of composition. Thus effort in the present study was focussed predominantly on the Riboud and Urbain models.

Model due to Riboud et al[13]

The slag constituents are classified in five different categories in this model. The mole fractions (x) for those categories being given by
(i) $x("SiO_2") = x(SiO_2) + x(PO_{2.5}) + x(TiO_2) + x(ZrO_2)$
(ii) $x("CaO") = x(CaO) + x(MgO) + x(FeO) + x(FeO_{1.5})$
(iii) $x(Al_2O_3)$
(iv) $x(CaF_2)$ and
(v) $x("Na_2O") = x(Na_2O) + x(K_2O)$.

The parameters A and B of equation 2) are calculated from the mole fraction of the five categories by using equations 3) and 4).

$$A = \exp(-19.81+1.73x("CaO")+5.82x(CaF_2)+7.02x(Na_2O)-33.76x(Al_2O_3)) \quad 3)$$

$$B = +31140-23896x("CaO")-46356x(CaF_2)-39159x("Na_2O")+68833x(Al_2O_3) \quad 4)$$

Subsequently, from the values of A and B it is possible to calculate the viscosity for the temperatures in question by use of equation 2).

Model due to Urbain et al[18]

In this model the parameters A and B are calculated by dividing the slag constituents into three categories (i) "glass formers", $x_G = x(SiO_2) + x(P_2O_5)$ (ii) "modifiers", $x_M = (CaO) + x(MgO) + x(Na_2O) + x(K_2O) + 3x(CaF_2) + x(FeO) + x(MnO) + 2x(TiO_2) + 2x(ZrO_2)$ (iii) "amphoterics", $x_A = x(Al_2O_3) + x(Fe_2O_3) + x(B_2O_3)$.

However we consider that Fe_2O_3 behaves more like a modifier than an amphoteric and in our revised programme $1.5\ x(FeO_{1.5})$ has been added to x_M and $x(Fe_2O_3)$ deducted from x_A. "Normalized" values x_G^* and x_M^* and x_A^* are obtained by dividing the mole fractions, x_G, x_M and x_A by the term $(1 + 2x(CaF_2) + 0.5\ x(FeO)_{1.5}) + x(TiO_2) + x(ZrO_2))$. Urbain proposed that the parameter B was influenced both by the ratio, $\beta = [x_M^*/(x_M^* + x_A^*)]$ and by x_G^*. The parameter B can be expressed in the form of equation (5) where B_1, B_2 and B_3 can be obtained by equation (6).

$$B = B_o + B_1\ x_G^* + B_2(x_G^*)^2 + B_3(x_G^*)^3 \quad 5)$$

$$B_i = a_i + b_i\beta + c_i\beta^2 \quad 6)$$

B_o, B_1, B_2 and B_3 can be calculated from the equations listed in Table 1 and these parameters are then introduced into equation 5) to calculate B. The parameter A can be calculated from B by equation 7) and the viscosity of the slag (in PaS) can then be determined using equation 8).

$$-\ln A = 0.2693\ B + 11.6725 \quad 7)$$

$$\eta = 0.1[AT \exp(10^3\ B/T)] \quad 8)$$

TABLE 1

$B_o = 13.8 + 39.9355\beta - 44.049\beta^2$
$B_1 = 30.481 - 117.1505\beta + 129.9978\beta^2$
$B_2 = -40.9429 + 234.0486\beta - 300.04\beta^2$
$B_3 = 60.7619 - 153.9276\beta + 211.1616\beta^2$

Modifications to the Urbain model

Urbain[18] has recently modified the model to calculate separate B values for different individual modifiers, CaO, MgO and MnO. The global B value for a slag containing all three oxides can be derived using equation 9)

$$B(\text{global}) = \frac{x(CaO)B(CaO) + x(MgO)B(MgO) + x(MnO)B(MnO)}{x(CaO) + x(MgO) + x(MnO)} \qquad 9)$$

Assessment of the viscosity models

These two models have been used to calculate the viscosities of slags with widely-varying compositions and it has been found that both give values which agree well with experiment.

The model of Urbain gives a slightly better fit than the Riboud model. The discrepancies between the experimental values and the predicted values are of the order of $\pm$ 30% which are of similar magnitude to the experimental uncertainties for viscosity measurements.

2.3 Density (ρ)

Recently Keene[25] has reported that the density at 1673K of molten slags can be obtained within $\pm$ 5% using the equation 10)

$$\rho\ /gcm^{-3} = 2.46 + 8.018\ (\%\ FeO + \%\ Fe_2O_3 + \%\ MnO + \%\ NiO) \qquad 10)$$

An additive method for the estimation of densities (ρ) in slags has been widely used for some time[26,27]. In this method, the molar volume, V, can be obtained from equations 11) and 12) below, where M, x and $\bar{V}$ are the molecular weight, mole fraction and the partial molar volume, respectively, and 1, 2 and 3 denote the various oxide constituents of the slag.

$$V = M_1x_1 + M_2x_2 + M_3x_3 \qquad 11)$$

$$V = x_1\bar{V}_1 + x_2\bar{V}_2 + x_3\bar{V}_3 \qquad 12)$$

The partial molar volume is usually assumed to be equal to the molar volume of the pure component (V^o). Bottinga and Weill[28] produced a series of values of $\bar{V}$ for various oxides assuming a constant value for $\bar{V}(SiO_2)$ and it was claimed that good estimations of the density could be obtained for compositions containing between 40 and 80% SiO_2. Two more recent studies[29,30] also concluded that $\bar{V}(SiO_2)$ was independent of composition and have revised the $\bar{V}$ values for the various oxides. However it has been pointed out[31,32] that the density of the slag is also related to its structure. Silicate slags contain a mixture of chains, rings and basic silicate units, which are dependent upon the silica concentration and upon the nature of the cations present. Thus the densities of silicate slags estimated using a constant value for $\bar{V}(SiO_2)$ will be subject to error as the arrangement of these silicate chains varies with silica concentration.

Furthermore Grau and Masson[31] pointed out that for the series M_2O, M_2SiO_2 the partial molar volume of SiO_2 is not constant. They calculated a $\Delta\bar{V}$ term for the differences between any two members of the series and in this way calculated values were derived for the systems FeO + SiO_2, PbO + SiO_2, FeO + MnO + SiO_2 and FeO + CaO + SiO_2 for compositions in the range x_{SiO_2} = 0.5 to 1.0. However this method is not suitable for calculating densities of multicomponent systems.

Very recently, Bottinga et al[33] have presented a model in which the partial molar volumes of alumina-silicate liquids were considered to be composition-dependent.

New model for calculating the densities of slags

Slags containing SiO_2, Al_2O_3 and P_2O_5 consist of chains, rings and complexes which are dependent upon the amount and nature of the cations present. Thus it is necessary to make the partial molar volumes dependent upon composition for oxides of this type. If in a binary system, equation 12) were applicable and if $\bar{V}_i = V_i^o$ ie. $\bar{V}$ is independent of composition, then the curve of V as a function of composition will be that shown by the solid line in Figure 1a and the two $x_1\bar{V}_i$ contributions by the dotted lines. If we now consider a binary silicate system the molar volume (V) would have the form shown as a solid line in Figure 1b. It is reasonable to assume that $\bar{V}(M_xO)$ is independent of composition and would have the form of $x_1\bar{V}_1$ in Figure 1b. The parameter $x_2\bar{V}_2$ can be derived for SiO_2 by use of equation 13) below.

$$x_2\bar{V}_2 = V - x_1\bar{V}_1 \qquad 13)$$

Thus $x_2\bar{V}_2$ will have the form of the curve shown in Figure 1b.

It is possible to derive $x\bar{V}$ for SiO_2 in ternary and quaternary slags by using equation 14). Values for $x\bar{V}(SiO_2)$ have been derived using experimental density data for the systems, $FeO + SiO_2$, $CaO + SiO_2$, $MnO + SiO_2$, $Na_2O + SiO_2$, $K_2O + SiO_2$ and $CaO + FeO + SiO_2$ and are plotted against $x(SiO_2)$ in Figure 2. It can be seen from this figure that there is excellent agreement between the $x\bar{V}(SiO_2)$ calculated from different sources, with the exception of that for the $MnO + SiO_2$ system; however the reliability of the experimental data for this system, have been questioned previously. From this curve for $x\bar{V}(SiO_2)$ we can derive the relationship, $V(SiO_2) = 19.55 + 7.966.x(SiO_2)$. The recommended values for $\bar{V}$ for the various oxides at 1500°C are given in Table 2.

$$xV(SiO_2) = V - x_1\bar{V}_1 - x_2\bar{V}_2 - x_3\bar{V}_3 \qquad 14)$$

Values for $x\bar{V}(Al_2O_3)$ were determined in a similar manner by using experimental density data for the systems, $CaO + Al_2O_3$, $CaF_2 + Al_2O_3$, $CaF_2 + Al_2O_3$, $SiO_2 + Al_2O_3$, $MgO + CaO + Al_2O_3$ and $MnO + SiO_2 + Al_2O_3$. The $xV(Al_2O_3)$ results are plotted in Figure 3 and the relationship $\bar{V}(Al_2O_3) = 28.31 + 32\,x(Al_2O_3) - 31.45\,x^2(Al_2O_3)$ was derived from this curve.

There are few experimental data for the density of phosphate slags, $x\bar{V}(P_2O_5)$ values were derived from data for the systems $CaO - FeO - P_2O_5$ and $Na_2O - P_2O_5$. A constant value of $\bar{V} = 65.7\ cm^3\ mol^{-1}$ was obtained from the selected linear relationship.

TABLE 2

Recommended values for the partial molar volumes, $\bar{V}$, of various slag constituents at 1500°C

SiO_2	$19.55 + 7.966\,x(SiO_2)$	FeO	15.8	K_2O	51.8
Al_2O_3	$28.31 + 32\,x(Al_2O_3) - 31.45\,x^2(Al_2O_3)$	Fe_2O_3	38.4	CaF_2	31.3
CaO	20.7	MnO	15.6	P_2O_5	65.7
MgO	16.1	Na_2O	33	TiO_2	24

Units of $\bar{V} = cm^3\ mol^{-1} = 10^{-6}\ m^3\ mol^{-1}$

In order to provide a temperature coefficient, the temperature dependencies of

the molar volumes (dV/dT) of many slag systems were examined and a mean value of 0.01% K^{-1} was adopted.

Assessment of density models.

An analysis of the uncertainties associated with the estimated of densities with this model has not been completed yet. However on the basis of those values obtained so far the standard deviation of the factor $[(\rho_{est}-\rho_{expt}/\rho_{expt}]$ is between 1 and 2% and less than that recorded vary the method due to Bottinga et al[33]. The experimental uncertainties associated with density measurements for slags are i.e. $\pm$ 2%.

2.4 Surface tension (γ)

Methods for estimating the surface tension of slags based on the addition of the partial molar contributions ($\bar{\gamma}$) of the individual constituents have been reported by Appen[34] by Boni and Derge[35] and by Popel[36]. All these methods make use of equation 13a where 1,2,3 etc denote the various slag constituents.

$$\gamma = x_1\bar{\gamma}_1 + x_2\bar{\gamma}_2 + x_3\bar{\gamma}_3 + \ldots\ldots \qquad 13a)$$

Values of $\bar{\gamma}_i$ are often taken to be the surface tension of the pure components, γ_i^o, and have also been obtained by reiterative procedures. Figure 4a shows a typical plot of γ as a function of x for a binary slag and the individual $x_i\bar{\gamma}_i$ contributions have been included These methods work well for certain slag mixtures but break down when surface-active constituents, such as P_2O_5, are present. Surface active components migrate preferentially to the surface and cause a sharp decrease in the surface tension and only very small concentrations are required to cause an appreciable decrease in γ if the constituent is concentrated in the surface layer. Thus some unreported or undetected impurity could have a marked effect on the surface tension of the slag and consequently produce an apparent error in the value estimated by the model. In this aspect surface tension differs from all the other physical properties which are essentially bulk properties.

Model for calculating the surface tension of slags

Figure 4a shows the surface tension of two slag constituents which are not surface active. For a binary mixture with one surface active component the surface tension-composition relationship will have the form of that shown in Figure 4b where 2 denotes the surface-active constituent. If we assume that $x\bar{\gamma}$ for component 1 is unaffected then the term $\bar{\gamma}_2 x_2$, the partial molar contribution of the surface active material, can be calculated by equation 14a below. The term $(x_2\bar{\gamma}_2)$ can similarly be calculated for ternary and quaternary systems providing there is only one surface active component. The compositional dependence of the $(x_2\bar{\gamma}_2)$ term is shown in

$$x_2\bar{\gamma}_2 = \gamma - x_1\bar{\gamma}_1 \qquad 14a)$$

Figure 4b and it should be noted that as $x_2 \longrightarrow 1$ then $x_2\bar{\gamma}_2 \rightarrow \gamma_2^o$. Values of $(x\bar{\gamma})$ for various surface active materials derived from experimental surface tension data are shown in Figures 5a. It is possible to deal with the compositional dependence of these $(x\bar{\gamma})$ values by considering two curves viz. one operating up to the point N and the other representing values of x where x > N. The partial surface tension for non-surface active constituents is shown in Table 3 and the equations for calculating $\bar{\gamma}$ for surface active components and values of N are given in Table 4. There is a considerable discrepancy in the $x_2\bar{\gamma}_2 - (x_2)$ relationships for B_2O_3 obtained from experimental data on two different systems,

consequently a mean value has been adopted until further data become available.

TABLE 3
Partial molar surface tension, $\bar{\gamma}$, at 1500 °C
for different slag constituents

Oxide	SiO_2	CaO	Al_2O_3	MgO	FeO	MnO	TiO_2
$\bar{\gamma}$/mNm^{-1}	260	625	655	635	645	645	360

TABLE 4
Values of $x_i\bar{\gamma}_i$ at 500°C for surface-active constituents

Slag Constituent	$x_i\bar{\gamma}_i$ for x < N	N	$x_i\bar{\gamma}_i$ for x > N
Fe_2O_3	$-3.7 - 2972\,x + 14312\,x^2$	0.125	$-216.2 + 516.2\,x$
Na_2O	$0.8 - 1388\,x - 6723\,x^2$	0.115	$-115.9 + 412.9\,x$
K_2O	$0.8 - 1388\,x - 6723\,x^2$	0.115	$-94.5 + 254.5\,x$
P_2O_5	$-5.2 - 3454\,x + 22178\,x^2$	0.12	$-142.5 + 167.5\,x$
B_2O_3	$-5.2 - 3454\,x + 22178\,x^2$	0.10	$-155.3 + 265.3\,x$
Cr_2O_3	$-1248\,x + 8735\,x^2$	0.05	$-84.2 + 884.2\,x$
CaF_2	$-2 - 934\,x + 4769\,x^2$	0.13	$-92.5 + 382.5\,x$
S	$-0.8 - 3540\,x + 55220\,x^2$	0.04	$-70.8 + 420.8\,x$

The reported values of $(d\gamma/dT)$ for various slag systems were examined and a mean value of -0.15 mN m^{-1} K^{-1} was applied as a temperature coefficient.

Assessment of the model

The standard deviation of the factor $[(\gamma_{est} - \gamma_{expt})/\gamma_{expt}]$ was ca. $\pm$ 10%. Undoubtedly much of the uncertainty arises from experimental errors, where the effect of unreported surface active impurities and the nature of the gaseous atmosphere could have a marked effect on the value of surface tension.

Another major source of error is the amount of Fe_2O_3 present in the slag, this investigation has shown clearly that Fe_2O_3 is very surface active. Few investigators cite the (Fe^{3+}/Fe^{2+}) ratio which in turn is dependent upon, (i) p_{O_2} (ii) T and (iii) the nature and amount of other oxides present and furthermore the ratio, when quoted, is vulnerable to error. Thus the problem arises if a decrease in γ is recorded when Na_2O is added to the slag, is this decrease due to a increase in Fe_2O_3 content or due to the surface activity? In this investigation attempts were made to compensate γ for an increase in Fe_2O_3 content but the effects of basic oxides on the Fe distribution are not well documented and some error may ensue.

A major unresolved problem concerns the situation where the slag contains more than one surface active component. It is possible that there is some competition for sites on the surface and hence the decrease in γ would not be as sharp as that calculated from the summation of $(x_A\bar{\gamma}_A + x_B\bar{\gamma}_B)$ where A and B denote surface active constituents. In this case the model may overestimate the decrease in γ. There are no extant data to confirm this possibility, we have, however, considered $(Na_2O + K_2O)$ as one contribution in the model.

2.5 Thermal Properties

The computation of the thermal losses in the converter by conductive and radiative processes requires knowledge of the following thermal properties, heat capacity, enthalpy, thermal conductivity, absorption coefficient and emissivity.

2.5.1 Heat capacity C_p and enthalpy $(H_T - H_{298})$ of slags

When a silicate liquid is cooled the structure of the solid formed is dependent upon the cooling rate and the thermal history of the sample. Consider a liquid at a temperature corresponding to the point C in Figure 6, a rapid quench will produce a glass and the enthalpy evolved will follow the path CLGA. By contrast, a very slow cooling rate will result in the formation of a crystalline slag, the enthalpy evolution following the path CL DB. It will be noted from Figure 6 that $(H_T - H_{298})_{cryst} = (H_T - H_{298})_{glass} + \Delta H^{vit}$, where ΔH_{vit} is enthalpy of the endothermic transformation of (crystal $\longrightarrow$ glass). The C_p values for the various phases can be summarized as:

$$C_p(\text{crystal}) \simeq C_p(\text{glass}) < C_p(\text{supercooled liquid}) \simeq C_p(\text{liquid})$$

It can be seen from Figure 6 that at the glass temperature (T_{gl}) there is a sudden increase in C_p (ΔC_p^{gl}) as the glass transforms into a supercooled liquid. Drop calorimetry studies on the glass phase at temperatures between T_{gl} and T_{liq} will produce progressively more crystallization as T_{liq} is approached and consequently the $(H_T - H_{298})$ - T relationship will be similar to that depicted by the dots in Figure 6 and not the path, AGLC; the magnitude of the apparent enthalpy of fusion (ΔH^{fus}) will be dependent upon the fraction of the sample crystallized during annealing at temperatures between T_{gl} and T_{liq}. The C_p values for the liquid and supercooled liquids have been reported[37] to be constant and independent of temperature. It follows from the triangle GEL in Figure 6 that $\Delta C_p^{gl}(T_{liq} - T_{gl}) = \Delta H^{fus}$. Thus it is possible to estimate the enthalpy of a slag with a glassy structure from estimates of C_p(glass) C_p(liq) and T_{gl}. However the estimation of T_{gl} is difficult as it can vary between ~ 700 and 1100 K and the various estimation rules suggested are known to be prone to appreciable errors[38]. Inspection of literature data[38,39] indicates that the glass transformation occurs when C_p attains a value of ca. 1.1 J K^{-1} g^{-1}; this rule has been used in the development of the following model for the estimation of $(H_T - H_{298})$ and C_p of slags with a glassy structure.

The C_p for glass, liquid and supercooled liquid phases can be estimated from the slag composition using partial molar heat capacities ($\bar{C}_p$) as shown in equation 15).

$$C_p = x_1\bar{C}_{p_1} + x_2\bar{C}_{p_2} + x_3\bar{C}_{p_3} + x_4\bar{C}_{p_4} \ldots \qquad 15)$$

For most materials the temperature dependence of C_p is usually expressed the form given by equation 16) where a, b and c are constants

$$C_p = a + bT - c\,T^{-2} \qquad 16)$$

The enthalpy at T relative to 298 K (25 °C) is obtained from equation 17) for the glass phase

$$(H_T - H_{298}) = \int_{298}^{T} Cp = a(T-298) + \frac{b}{2}(T^2 - 298^2) + \frac{C}{T} - \frac{C}{298} \qquad 17)$$

Values of a, b and c for the various slag components are given in Table 5 and it should be noted that the P_2O_5 and S in the slag were calculated as CaP_2O_6 and $CaSO_4$, respectively. The amount of CaO used in the calculation of $x\bar{C}_p$(CaO) should be adjusted by the relationship x(CaO) = x(CaO ,total) - x(P_2O_5) - x(S) to account for the CaO in CaP_2O_6 and $CaSO_4$. The model also takes into account the presence of free iron in the slag.

TABLE 5

Slag Component	M	$\bar{C}_p$(glass)/calK^{-1}mol^{-1}=a+bT -c/T^2 a	b.10^3	c.10^5	$\bar{C}_p$(liq) cal K^{-1}mol^{-1}
SiO_2	60.09	13.38	3.68	3.45	20.79
CaO^2	56.08	11.67	1.08	1.56	19.3
Al_2O_3	101.96	27.49	2.82	8.4	35
MgO^3	40.31	10.18	1.78	1.48	21.6
K_2O	94.2	15.7	5.4	0	17.7
Na_2O	61.98	15.7	5.4	0	22
TiO_2	79.9	17.97	0.28	4.35	26.7
MnO^2	70.94	11.11	1.94	0.88	19.1
FeO	71.85	11.66	2.0	0.67	18.3
Fe_2O_3	159.7	23.49	18.6	3.55	45.7
Fe^3	55.85	3.04	7.58	-0.6	10.5
P_2O_5	141.91	43.63	11.1	10.86	58
CaF_2	78.08	14.3	7.28	-0.47	23
SO_3^2	80.06	16.78	23.6	0	42

1 cal = 4.184 J; T in K

The values of $\bar{C}_p$ for the liquid and supercooled liquid given in Table 5 are those reported by Carmichael et al[40] except $\bar{C}_p$ values for Al_2O_3 and Fe_2O_3, where other values have been preferred.

Thus ($H_T - H_{298}$) values for a liquid slag at temperature T can be estimated by determining T_{gl} (ie temperature at which C_p = 1.1 J K^{-1} g^{-1}) and calculating ($H_{T_{gl}} - H_{298}$) from equation (17) and ($H_T - H_{T_{gl}}^p$) from C_p(liq).($T-T_{gl}$).

Values of C_p(glass) obtained with this model lie within 2% of the experimental values and the C_p(liq) values also appear to agree with experimental data; values of ΔC_p at T_{gl} calculated using the model lie within the range of experimental values[38,39] of 0.15 to 0.30 J K^{-1} g^{-1}. One major uncertainly would appear to lie in the calculation of T_{gl}, however it can be shown that an error in T_{gl} of 100 K would only produce an error of ca. 1% in the value of ($H_{1900} - H_{298}$) for the slag. The most serious source of error would thus appear to arise through crystallization of the sample during quenching, as few data are available for ΔH^{vit}, the magnitude of errors arising from this source have not been evaluated.

2.5.2 Heat transfer in slags

Heat is transferred through slags by a variety of mechanisms which include convection, radiation and various thermal conduction processes, viz. thermal ("phonon") conductivity, (k_c), electronic conductivity (k_{el}) and radiation conductivity (k_R). Methods for estimating the various physical properties involved in these processes are considered below.

2.5.3 Thermal conductivity (k)

Heat is transferred by phonons which are quanta of energy associated with each mode of vibration in the sample. Scattering of the phonons causes a decrease in the thermal conductivity and thus the conductivity is sensitive to the structure of the slag and consequently those factors affecting structure such as the basicity. Despite this structure dependence, estimation rules based on the additivity principle (equation 18)) have been proposed[41,42]. Other models have been developed which relate k to the volume concentration of the oxides in the

glass[43] and a third approach[44] relates the thermal resistance (1/k) to $x_i m_i$ where m_i is the effectiveness of modifier of component i in scattering phonons.

$$k = (\%i)k_i + (\%j)k_j + \ldots\ldots \quad 18)$$

However in coal slags there is frequently an appreciable degree of crystallization and the thermal conductivity value varies with the thermal history of the sample[45], and consequently rules developed for glasses may not apply well for coal slags. Recent work carried out on a large number of silicate slags[46] indicated that the thermal diffusivity, a, ($a=k/C_p.\rho$) of various slags was independent of both composition and temperature in the range (500-1300 K) with $a(glass) = 4.5(\pm 0.5)\times10^{-7}\ m^2s^{-1}$; $a(cryst) = 6\times10^{-7}\ m^2s^{-1}$ and $a(liq) \simeq a(glass)$. These data are consistent with values reported for coal slags[45] and steelmaking slags[47]. However, the values reported by Nauman et al[48] indicate that at high FeO contents (> 20%) both k and a increase with increasing FeO content ($k = 0.8 + 1.7\times10^{-2}$(% FeO) $Wm^{-1}K^{-1}$).

2.5.4 Absorption coefficient (α)

Radiation conductivity (k_R) can be the predominant mode of heat transfer through semi-transport media like glasses and the magnitude of k_R is determined largely by the optical properties such as the absorption coefficient (α) and the refractive index (n). The value of k_R increases as the slag thickness (d) is increased until a critical point is attained, above this point k_R remains constant and independent of thickness. Above this critical point the slag is said to be "optically thick, this condition applies when $\alpha d > 3.5$ and values of k_R can be calculated using equation 19), where σ is the Stefan-Boltzmann constant.

$$k_R = \frac{16\, n^2 T^3 \sigma}{3\alpha} \quad 19)$$

No formulae exist for the calculation of k_R for optically thin conditions. The absorption coefficient (α)[49] is markedly dependent upon the amounts of Fe^{2+} and Mn^{2+} present in the slag; levels for FeO < 5% the following relationship can be applied, $\alpha(cm^{-1}) = 11(\%FeO)$. Temperature appears to have little effect on the absorption coefficient of glasses but the absorption coefficients of magmas have been reported to increase with increasing temperature[50,51]. Crystallization of the slag will result in a large increase in the absorption (or extinction) coefficient which could reduce k_R to virtually zero.

The importance of radiation conduction in heat transfer through coal slags can readily be demonstrated, for a slag with an appreciable FeO content (7%) Fine et al[47] recorded $\alpha \simeq 50\ cm^{-1}$ at 298 K using this value and equation 19), a value of $k_R = 0.9\ Wm^{-1}K^{-1}$ can be calculated for 1873 K. As $k_c \simeq 1.5\ Wm^{-1}K^{-1}$ it can be seen that about 40% of the heat is transferred by radiation conduction.

2.5.5 Emissivity (ε)

The emissivity (ε) of a semi-transparent medium, is a bulk property cf. ε (metal) which is solely dependent upon the surface. In the basis of the spectral and total normal emissivity data reported for coal and metallurgical slags the value $\varepsilon = 0.8 \pm 0.1$ can be adopted for coal slags in the range (1100 - 1900 K).

CONCLUSIONS

1) Estimation procedures based on the chemical composition of the slag have now been developed for the prediction of viscosity, surface tension, density and heat capacity.
2) The accuracy of these estimation routines for some physical properties (eg viscosity, surface tension) can be improved when more reliable experimental data become available.
3) The distribution of iron in the slag betwen free Fe, FeO and Fe_2O_3 has a pronounced effect of virtually all the physical properties and it is recommended that experimental data for the properties of the slag should always be accompanied by values for the distribution of iron.
4) The development of models for the prediction of some physical properties (thermal conductivities, absorption coefficient) is restricted by the limited amount of experimental data available.

REFERENCES

1) DARKEN, L.S. and GURRY, R.W. J. Am. Chem. Soc. 1946, 68, 798.

2) LARSON, H. and CHIPMAN, J. J. Metals, 1953, Sept., 1089.

3) BANYA, S. and SHIM, J.D. Canad. Metall. Q., 1982, 21, 319.

4) SONDREAL, E.A. and ELLMAN, R.C. Fusibility of ash from lignite and its correlation with ash composition. US Energy Res. and Develop. Admin. GFERC/RI-75-1, Pittsburgh, 1975.

5) WINEGARTNER, E.C. and RHODES, B.T. J. Eng. Power, 1975, 97, 395.

6) BRYERS, R.W. and TAYLOR, T.E. J. Eng. Power, 1976, 98, 528.

7) STEILER, J.M. Commission of the European Communities Research Contract, 7210 CA/3/3/03. Thermodynamic data for steelmaking. 1981, Eur N7820, BP 1003, Luxembourg 1982.

8) GAYE, H. Ironmaking and Steelmaking, 1984, in press.

9) GAYE, H. Paper presented at Metallurgical Conference, Centenary of Teaching of Metallurgy, held at Strathclyde University, 25/26 June 1984.

10) OCHOTIN, M.W. Steklo Keram., 1954, 11, 7.

11) LYON, K.C. J. Res. Natl. Bur. Stand., 1974, 78, 497.

12) MCCAULEY, W.D. and APELIAN, D. Canad. Metall. Quart., 1981 20, 247.

13) RIBOUD, P.V., ROUX, Y, LUCAS, L.D. and GAYE, H. Fachber. Huttenpraxis Metallveiterverarb., 1981, 19, 859.

14) MAIRY, B. Private communication, Centre Recherches Metallurgique, Liege, Belgium.

15) BOTTINGA, Y. and WEILL, D.F. Am. J. Sci., 1972, 272,

16) SHAW, H. Am. J. Sci., 1972, 272, 870.

17) URBAIN, G., CAMBIER, F., DELETTER, M. and ANSEAU, M.R. Trans. J. Brit. Ceram. Soc., 1981, 80, 139.

18) URBAIN, G. Private communication, CNRS, Laboratoire de Ultra-Refractaires, Odeillo, France. Jan. 1983.

19) WATT, J.D. and FEREDAY, D. J. Instr. Fuel, 1969, 338, 99.

20) BOKAMP, . Inst. of Gas Technol. Preparation of a coal conversion systems Technical Data Book. Energy Res. and Dev. Admin. Report FE-1730-21 (1976).

21) CAPPS, W. and KAUFFMAN, D. Natl. Bur. Stand. Quart. Prog. Rept. to Office of Coal Res., Dept. Interior, 30/9/74.

22) SCHOBERT, H.H. Div. Fuel Chem. Prep., 1977, 22, 143.

23) SCHOBERT, H.H. and WITTHOEFFT, C. Fuel Proc. Technol., 1981, 5, 157.

24) HENSLEE, S.P. and KELSEY, P.V. Jr. US Dept. of Energy Report, EGG-FM-6049, Sept. 1982.

25) KEENE, B.J. National Physical Laboratory Report, DMA(D)75, Feb. 1984.

26) MOREY,G.H. Properties of Glasses. Rienhold,New York,1954,217.

27) HUGGINS,M.L;SUN,K.H. J.Am.Ceram.Soc. 1948,26,4.

28) BOTTINGA, H. and WEILL, D.E. Am. J. Sci., 1972, 272 438.

29) NELSON, S.A. and CARMICHAEL, I.S.E. Contrib. Mineral Petrol, 1979, 71, 117.

30) MO, Y., CARMICHAEL, I.S.E., RIVERS, M. and STEBBINS, J. Mineralog. Mag., 1982, 45, 237.

31) GRAU, A.E. and MASSON, C.R. Canad. Metall. Quart., 1976, 15, 367.

32) LEE, Y.E., GASKELL, D.R. Metall. Trans., 1974, 5, 853.

33) BOTTINGA, Y., WEILL, D.E. and RICHET, P. Geochim Cosmochim. Acta, 1982, 46, 909.

34) APPEN, A.A., SHISHKOV, K.A. and KAYALOVA, S.S. Zhur. Fiz. Khim, 1952, 26, 1131.

35) BONI, R.E. and DERGE, G. J. Metals, 1956, 8, 53.

36) POPEL, S.E. Metallurgy of slags and their use in building. 1962, 67.

37) RICHET, P. and BOTTINGA, Y. Geochim. Cosmochim Acta, 1984, 44, 1533.

38) BACON, C.R. Am. J. Sci., 1977, 277, 109.

39) MOYNIHAN, C.T., EASTEAL, A.J., TRAN, D.C., WILDER, J.A. and DONOVAN, E.P. J. Am. Ceram. Soc., 1976, 59, 137.

40) CARMICHAEL, I.S.E., NICHOLLS, J., SPERA, F.J., WOOD, B.J. and NELSON, S.A. Phil. Trans. Roy. Soc. (London), 1977, A286, 373.

41) MOREY, G.W. Properties of Glass. Reinhold, New York, 1954, 217.

42) ABAKOVA, I.G. and SERGEEV, O.A. Thermophysical properties of glasses. Proc. of Metrological Inst. of USSR, No.129 (189), Moscow-Leningrad, 1971, 13.

43) MISNAR, A. Thermal conductivity of solid, gases and composite materials. Leningrad, 1968.

44) VAVILOU, Y.V., KOMAROV, V.E. and TABUNOVA, W.A. Phys. Chem. Glasses, 1982, 8, 472.

45) GIBBY, R.L. and BATES, J.L. 10th Thermal Conductivity Conf. held Newton, Mass. Sept. 1970, IV-7,8.

46) TAYLOR, R. and MILLS, K.C. Unpublished work, 1984.

47) FINE, H.A., ENGH, T. and ELLIOTT, J.F. Metall. Trans. B. 1976, 7B, 277.

48) NAUMAN, J., FOO, G. and ELLIOTT, J.F. Extractive Metallurgy of Copper. Chapter 12, 237.

49) STEELE, F.N. and DOUGLAS, R.W. Phys. Chem. Glasses, 1965, 6, 246.

50) FUKAO, Y., MITZUTANI, H. and UYEDA, S. Phys. Earth Planet Interiors, 1968, 1, 57.

51) ARONSON, J.R., BELLOTI, L.H., ECKROAD, S.W., EMSLIE, A.G., MCCONNELL, R.K. and THUNA, P.C., von. J. Geophys. Res., 1970, 75, 3443.

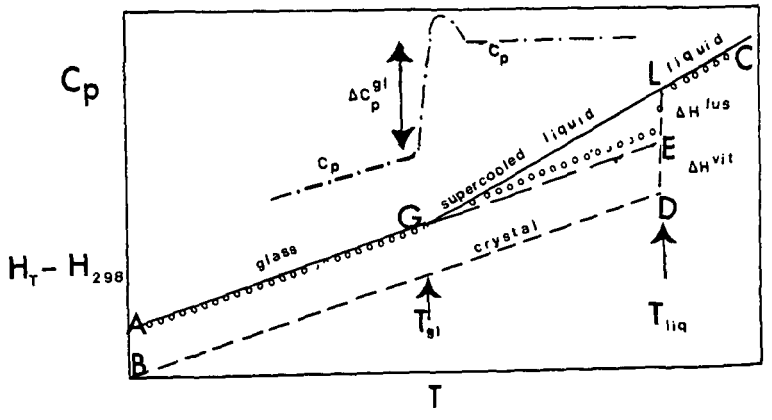

Figure 6 Cp and $(H_T - H_{298})$ for glassy and crystalline phases of a slag; O, indicates typical drop calorimetry results.

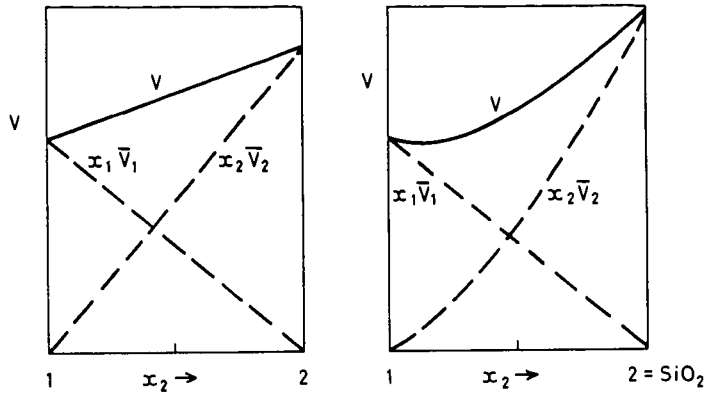

Figures 1a The molar volume of binary slag system as a function of composition and 1b. showing the individual $x_i\bar{V}_i$ contributions.

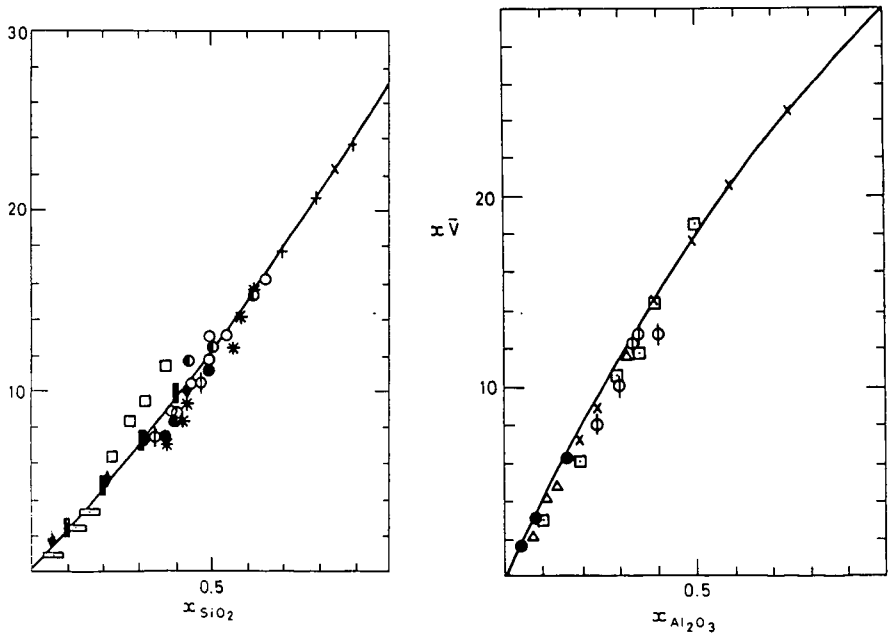

Figure 2. $x\bar{V}(SiO_2)$ as a function of $x(SiO_2)$

Figure 3. $x\bar{V}(Al_2O_3)$ as a function of $x(Al_2O_3)$

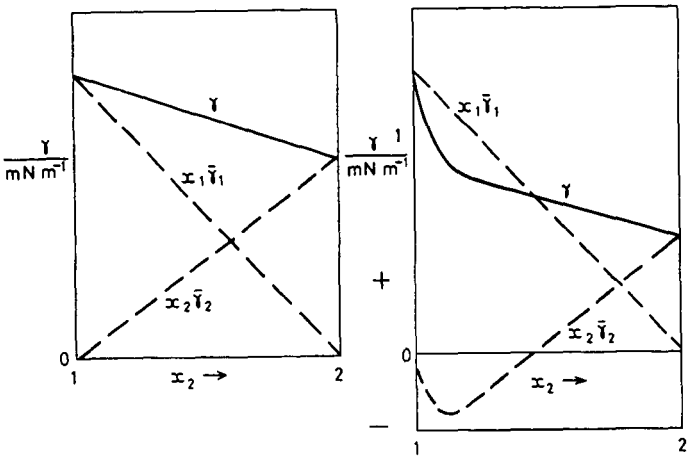

Figure 4a. The compositional dependence of , $x_1\bar{\gamma}_1$ and $x_2\bar{\gamma}_2$ for a binary slag system with non-surface active constituents

Figure 4b. with one surface active constituent (2).

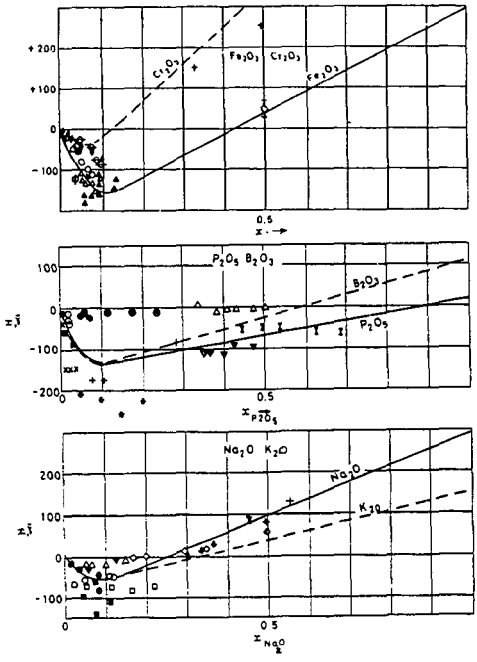

Figure 5 The compositional dependence of $x_i\bar{\gamma}_i$ for various surface-active constituents.

Viscosity of Fluxes for the Continuous Casting of Steel

W. L. McCauley and D. Apelian

Materials Engineering, Drexel University, Philadelphia, PA, 19104

Mold fluxes are routinely used in both continuous casting and bottom pouring of steel. These fluxes are generally calcium-silicate based compositions with alkali oxides [$(Li, Na, K)_2O$] and fluorides [CaF_2, NaF] added as fluidizers. The compositions are sometimes based on the blast furnace slag [Al_2O_3-SiO_2] system, but the fly ash [CaO-SiO_2] system is more common.

A variety of properties of the flux must be controlled, including fusion characteristics (fusion temperature range and sintering characteristics, flow properties of the powder, viscosity of the molten flux, and non-metallic absorption ability. The viscosity influences the consumption rate of flux, heat transfer in the mold, and non-metallic dissolution rate, and has been the subject of a great deal of published and unpublished work over the last ten years. The purpose of this paper is to discuss the expression of viscosity as a function of composition and temperature in separate relations.

In a previously published work (1), fluxes based on the CaO-SiO_2 system were examined to determine the effects of basicity ratio and alkali oxide and fluoride additions on the viscosity of oxide melts in the mold flux composition range. Those results showed that for that range of compositions, the viscosity at a given temperature could be expressed as a function of the silica content squared. In this work, an expression for viscosity as a function of temperature is derived from the Claussius-Clapeyron equation.

Previous Work - Viscosity vs. Composition

The viscosity of twenty controlled composition fluxes was measured as a function of temperature. The compositions, given in Table 1, were selected to fit a second order statistical design in the variables V-ratio, $\%Na_2O$ and $\%CaF_2$. The V-ratio [wt%CaO/wt%SiO_2] was varied from 0.6 to 1.3, Na_2O from 4 to 19wt%, and CaF_2 from 2 to 12wt%. Al_2O_3 was kept constant at 10wt%. The viscosity was measured using a rotating type viscometer with a molybdenum spindle in an argon atmosphere. Details of the experimental technique were reported earlier (1).

A summary of the experimental results is given in Table 2. Viscosity decreased with increasing V-ratio, CaF_2 content and Na_2O content as shown in Figures 1, 2 and 3, respectively. A plot of viscosity vs. silica content, Figure 4, shows that silica has a predominating effect on viscosity. A simple quadratic relation of viscosity with wt% silica or mole fraction of silicon cations produced a better fit of the data than a model containing the design variables. The best fit of data was obtained with a quadratic relation of the ratio of network forming cations [Si, Al and Zr] to total anion concentration [O and F]. Specifically,

$$\eta_{1500°C} = 6.338 - 43.44K + 75.03K^2$$

where

$$K = \frac{X_{Si} + X_{Al} + X_{Zr}}{X_O \quad X_F}$$

The log of viscosity versus reciprocal absolute temperature showed a distinct non-linearity as evidenced by the typical results shown in Figure 5. This is not a complete surprise, but a simple Arrhenius type equation is not adequate to describe the viscosity/temperature relationship.

Viscosity vs. Temperature

Viscosity can be considered as a measure of the ease of movement of molecules in a liquid undergoing shear. Several factors may influence this ease of movement including molecule size and intermolecular attraction, but a major factor is the amount of space available between the molecules, hence, the variety of models incorporating a free volume term.

The Claussius-Clapeyron equation relates pressure with temperature, enthalpy, and volume, and has been used to develop semi-theoretical expressions of vapor pressure (2). Many properties, including viscosity, can be related to an energy barrier, free volume and temperature. The attempt here is to express viscosity in the form of the Claussius-Clapeyron equation.

The Claussius-Clapeyron equation can be written

$$\frac{dP}{dT} = \frac{H}{T\,\Delta V} = \frac{\Delta H}{T(V-V_o)} \qquad 1)$$

where P, T, and ΔH have their usual meaning. For this discussion, ΔV is a measure of free volume or the difference between the volume at temperature and the volume at some standard state, e.g., at absolute zero.

Equation 1 can be rewritten as

$$\frac{d(\ell nP)}{d(1/T)} = -\frac{\Delta H}{R\,\Delta z} \qquad 2)$$

where $\Delta z = PV/RT - PV_o/RT$

Expanding ΔH to the Taylor series form and integrating with respect to 1/T yields

$$\ell nP = \frac{1}{R}\left(a - \frac{\Delta Ho}{T} + b\ell nT + dT + \frac{e}{2}T^2 + \ldots\right) \qquad 3)$$

If the higher order terms are ignored, the expression reduces to

$$\ell nP = A - \frac{B}{T} + C\ell nT \qquad 4)$$

Such a derivation was originally developed and used by Kirchoff [1858] and Rankine [1849] (2) to express the temperature dependence of vapor pressure. It was also successfully used by Brostow (3) to express the temperature dependence of the isothermal compressibility of a wide variety of organic liquids, some metallic liquids and water. By a similar analogy, we have used it to express the viscosity of liquid mold fluxes.

Regression Analysis

The flux viscosity data was fitted to the Kirchoff-Rankine equation as,

$$\eta = \exp(C_1 + \frac{C_2}{T} + C_3 \ell nT) \quad 5)$$

and to the Andrade-Arrhenius equation

$$\eta = A \exp(E/RT) \quad 6)$$

using the Marquardt method of non-linear least squares regression in the Statistical Analysis Systems [SAS] program package (4). The results of the regression are given in Table 3. The standard deviation and an average difference between calculated and measured values are given in Table 4.

In some cases, viz., Fluxes 5, 6 and 13 in Table 3, the signs of the coefficients are reversed, and a concave downward curve is generated. This is most likely caused by the regression being trapped at a local minimum in the data and assuming convergence at that point. It is required for these cases that the size of the regression step should be increased to avoid the local minima, which SAS does not allow. Also, there may not be enough data points to expand the regression step as is probably true for Fluxes 6 and 13.

For the majority of fluxes evaluated, the standard deviation, s, and the average percent variation, $\bar{\Delta}\%$, is lower for the Kirchoff-Rankine fitted equation vs. the Andrade-Arrhenius model, indicating a better fit of the experimental data. The average percent variation between calculated and experimental values is lower for the Kirchoff-Rankine equation, and the difference is most pronounced for those fluxes where the non-linearity of the experimental $\ell n\ \eta$ vs. $1/T$ data is greatest.

Discussion

When the non-linearity of the log viscosity vs. reciprocal temperature data was first observed, tests were made to insure that the curvature was real and not an artifact of the experimental apparatus. Hysteresis curves and constant temperature for extended time tests showed that the non-linearity was not caused by volatilization of alkali or fluoride constituents or from thermal deviations in the furnace setup. The observed curvature of the data was not an artifact and represented the true physical behavior of the materials. The application of the Kirchoff-Rankine equation produced a more accurate description of the temperature dependence of viscosity.

Additional work on liquid metals, simple chloride salts and some small molecule organic liquids (5) indicates that the advantage of the Kirchoff-Rankine equation over the Andrade-Arrhenius equation improves as the size of the melt species increases. The improvement in the description of viscosity vs. temperature for metals and simple salts [e.g., NaCl and $BiCl_2$] is not great, but for materials with larger melt species, there is a distinct improvement.

References

(1) W. L. McCauley and D. Apelian, *Canadian Metallurgical Quarterly*, 20(2) 1984, pp. 247-262.

(2) G. W. Thomson, *Chemical Review*, 38, February 1946.

(3) W. Brostow and P. Maynadier, *High Temperature Science*, 11 1979, pp. 7-21.

(4) SAS User's Guide, SAS Institute, Inc., Cary, North Carolina, 1979.

(5) W. L. McCauley and D. Apelian, "Temperature Dependence of the Viscosity of Liquids," to be presented at the International Symposium on Slags and Fluxes, TMS-AIME Fall Meeting, Lake Tahoe, NV, November 1984; to be published.

Table 1. Experimental Fluxes - Frit Composition, wt%

Flux	SiO_2	Al_2O_3	CaO	Na_2O	CaF_2	MgO	ZrO_2	Total	V-ratio
1	34.8	10.2	32.7	10.7	7.6	0.9	0.6	97.5	0.94
2	34.4	9.8	32.1	10.9	8.4	0.7	0.6	96.9	0.93
3	34.5	10.0	32.7	11.0	7.6	0.7	0.7	97.2	0.95
4	34.6	10.1	32.5	10.8	7.8	0.6	0.6	97.0	0.94
5	34.6	10.3	32.3	10.9	8.0	0.7	0.5	97.3	0.93
6	34.7	10.1	33.0	10.8	7.2	0.6	0.6	97.0	0.95
7	26.7	9.8	31.8	14.4	11.7	0.6	1.9	96.9	1.19
8	30.7	8.9	32.6	12.9	2.3	0.7	8.8	96.9	1.06
9	31.2	10.4	40.3	5.7	7.6	0.8	0.7	96.7	1.29
10	35.2	10.3	40.8	5.7	3.3	0.9	0.8	97.0	1.16
11	33.5	10.4	24.9	15.1	11.5	0.5	0.4	96.3	0.77
12	38.8	10.4	26.2	15.1	3.5	0.7	0.9	95.6	0.67
13	41.9	10.6	29.5	6.8	7.8	0.7	0.9	98.2	0.77
14	48.0	10.6	28.6	6.5	3.3	0.8	1.4	99.2	0.60
15	46.8	10.4	22.2	10.7	5.5	0.6	2.7	98.9	0.47
16	30.6	10.0	36.2	10.3	7.0	1.0	2.1	97.2	1.18
17	30.0	10.2	27.8	18.6	8.2	0.8	1.6	97.2	0.93
18	39.6	10.4	35.7	4.0	4.7	1.0	1.3	96.7	0.90
19	32.4	10.4	30.4	10.8	11.7	0.7	1.1	97.5	0.94
20	39.1	10.4	32.6	11.3	1.7	0.9	1.2	97.2	0.83

Table 2. Summary of Flux Viscosities

Flux	Viscosity at 1300°C, Ns m^{-2}	Viscosity at 1400°C, Ns m^{-2}	Viscosity at 1500°C, Ns m^{-2}
1	0.395	0.230	0.135
2	0.310	0.175	0.112
3	0.340	0.205	0.128
4	0.485	0.235	0.125
5	0.290	0.190	0.088
6	0.510	0.230	0.122
7	0.110	0.065	0.035
8	NA*	NA*	NA*
9	0.280	0.160	0.080
10	6.00	0.360	0.180
11	0.270	0.150	0.114
12	0.930	0.460	0.270
13	1.15	0.530	0.280
14	2.80	1.30	0.710
15	2.40	1.30	0.725
16	7.00	0.170	0.090
17	0.160	0.115	0.059
18	1.40	0.670	0.380
19	0.250	0.130	0.094
20	1.40	0.720	0.410

*Not available

Table 3. Regression Analysis Results

	Andrade-Arrhenius Equation				Kirchoff-Rankine Equation					
Flux	A (Pa s)	E (cal/mole)	s†	$\overline{\Delta\%}$††	C_1	C_2	C_3	s	$\overline{\Delta\%}$	n†††
1	8.831E-6	33783	7.03E-3	2.40	-184.35	51341	20.502	6.36E-3	1.94	12
2	2.704E-6	36304	1.99E-2	7.98	-282.59	68183	32.337	1.27E-2	3.47	6
3	2.332E-6	30095	8.92E-3	2.08	-184.30	47516	20.792	5.68E-3	1.42	6
4	8.016E-7	41748	1.82E-2	2.73	-278.11	71633	31.502	1.67E-2	3.20	6
5	2.528E-5	29493	2.15E-2	4.14	132.94	-10764	-17.290	2.10E-2	3.91	14
6	8.079E-7	41814	2.33E-2	5.41	123.80	-5309	-16.447	2.29E-2	5.68	7
7	1.963E-7	41439	1.31E-2	7.01	-1511.91	297516	179.394	5.72E-3	3.91	5
9	1.496E-5	30736	1.22E-2	3.15	-1626.10	321853	192.942	1.11E-2	3.62	6
10	7.5E-3	36000*	-	-	-8603.16	1735752	1019.0	2.83E-2	3.97	18
11	7.820E-6	32510	1.43E-2	3.15	-276.14	63473	31.935	5.81E-3	1.52	7
12	4.828E-7	45110	6.00E-2	2.95	-239.51	62253	27.155	3.35E-2	1.10	12
13	2.661E-6	40700	5.19E-2	4.69	169.80	-13879	-21.843	5.00E-2	3.89	8
14	5.488E-8	48579	2.26E-1	13.00	-987.72	212141	116.012	9.85E-2	5.30	11
15	5.761E-6	40568	1.32E-1	5.57	-233.90	60668	26.660	6.26E-2	3.07	10
16	2.0E-2	30000*	-	-	-42701.6	8456727	5071.8	8.69E-2	15.8	17
17	5.469E-6	32981	8.65E-3	5.05	-483.18	105664	56.221	1.60E-3	0.84	5
18	4.126E-6	39880	2.66E-2	3.01	-200.79	56382	22.457	1.66E-2	1.84	6
19	7.393E-6	32313	1.48E-2	7.39	-377.12	85334	43.656	8.69E-3	4.89	7
20	1.493E-7	50240	1.62E-1	16.46	-517.30	116706	60.246	5.32E-2	4.46	8

† $s = \sqrt{\epsilon(\eta^2_{exp} - \eta^2_{calc})/(n-1)}$

†† $\overline{\Delta\%} = \frac{1}{n}\left(\frac{\eta_{exp} - \eta_{calc}}{\eta_{exp}}\right) \times 100$

††† n = number of observations

* estimated

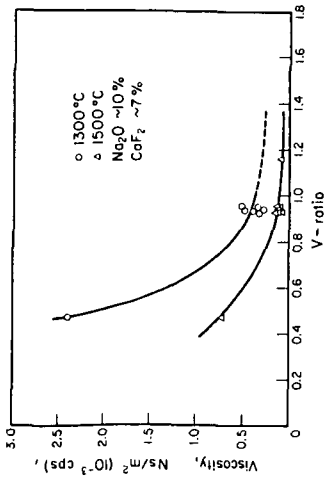

Figure 1. Viscosity vs. V-ratio

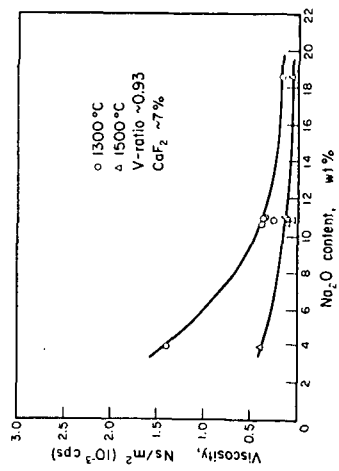

Figure 2. Viscosity vs. Na_2O Content

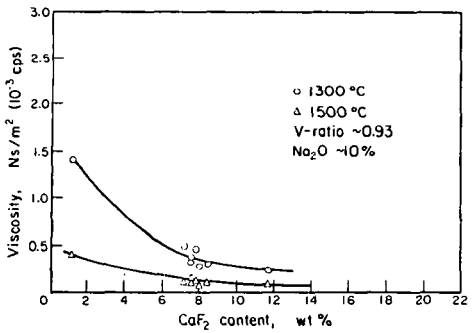

Figure 3. Viscosity vs. CaF_2 Content

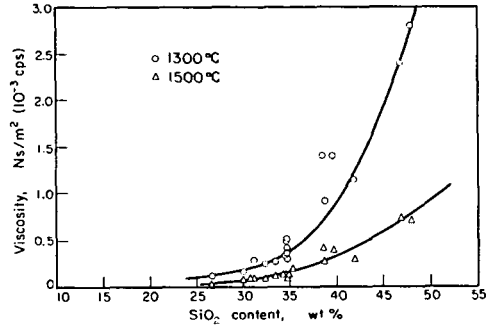

Figure 4. Viscosity vs. SiO_2 Content

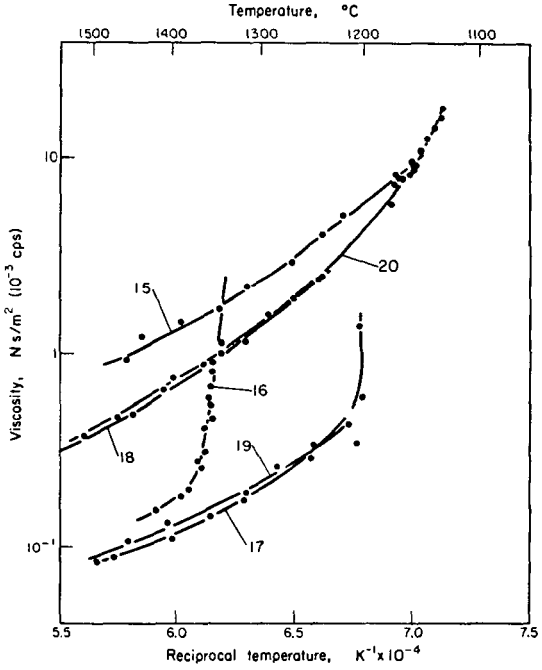

Figure 5. Typical viscosity results vs. reciprocal temperature

RHEOLOGICAL PROPERTIES OF MOLTEN KILAUEA IKI BASALT CONTAINING SUSPENDED CRYSTALS

H. C. Weed, F. J. Ryerson, and A. J. Piwinskii

University of California, Lawrence Livermore National Laboratory
Livermore, CA 94550

INTRODUCTION

In order to understand the flow behavior of molten silicates containing suspended crystals, we need to know the rheological behavior of the system as a function of volume fraction of the suspended crystalline phases at appropriate temperatures, oxygen fugacities and bulk compositions. This approach can be applied to magma transport during volcanic eruptions, large scale convective and mixing processes in magmatic systems, and fouling of internal boiler surfaces by coal ash slags in plants burning pulverized coal.

EXPERIMENTAL METHODS

We are currently determining the dynamic viscosity and crystallization sequence for a basalt from Kilauea Iki, Hawaii at 100 kPa total pressure. The oxygen fugacity is controlled by mixing CO and CO_2. The mixing proportions are chosen to yield oxygen fugacities corresponding to the high temperature extrapolation of quartz-fayalite-magnetite buffer (i.e. QFM, see Huebner (1)). Viscosities are being measured in an iron-saturated, Pt-30% Rh, rotating-cup viscometer of the Couette type from 1250° to 1150°C. The temperature interval for the crystallization sequence ranges from 1270° to 1130°C; the oxygen fugacity is maintained by flowing CO/CO_2 mixtures and is monitored by a ZrO_2 sensor cell. Low temperature limits on the investigated crystallization sequence are dictated by the sluggish kinetics encountered in this system.

RESULTS

The major element bulk composition of the starting material used in our experiments is given in Table 1:

TABLE 1. Analyses of Starting Material

Oxide	Kilauea Iki	Shaw et. al(2)
SiO_2	46.29	50.14
Al_2O_3	10.44	13.37
MgO	17.90	8.20
FeO*	11.34	10.13
Fe_2O_3	-	1.21
CaO	8.49	10.80
Na_2O	1.84	2.32
P_2O_5	0.22	0.27
K_2O	0.40	0.53
TiO_2	1.89	2.63
MnO	0.19	0.17
TOTAL	99.90	99.77

*All iron as FeO

The crystallization experiments were carried out employing a specimen of Kilauea Iki whole rock powder. The experimental results obtained at the QFM buffer are listed in Table 2. Olivine and chrome spinel are the only crystalline phases which occur between 1240°and 1179°C; clinopyroxene and plagioclase feldspar crystallize at approximately 1170°C.

Approximately 30 weight per cent crystallization occurs between 1250° and 1180°C. The liquid line of descent is characterized by a slight SiO_2, Al_2O_3 and alkali enrichment and an FeO and MgO depletion.

The volume percentage of melt as a function of temperature is shown in Figure 1. The break in slope at approximately 1170°C, corresponds to the appearance of clinopyroxene and plagioclase feldspar (see Table 2).

TABLE 2. Results of Selected Kilauea Iki Liquidus Experiments

Exp't No.	Time (Hrs)	Temp (°C)	Experiment Products	Vol % Melt[a]	Wt % Melt[b]
14	93.0	1240	olivine, chrome spinel, glass	71.8	78.1
9	189.5	1230	olivine, chrome spinel, glass	80.2[c]	76.1
8	24.0	1219	olivine, chrome spinel, glass	77.3	74.8
10	290.0	1209	olivine, chrome spinel, glass	76.2	74.2
12	289.0	1189	olivine, chrome spinel, glass	63.8	72.5
13	364.0	1179	olivine, chrome spinel, glass	71.8	71.5
16	380.0	1170	olivine, chrome spinel, clino-pyroxene, plagio-clase, glass	69.6	68.5
19	400.0	1160	olivine, chrome spinel, clino-pyroxene, plagio-clase, glass	54.7	53.5
20	400.0	1149	olivine, chrome spinel, clino-pyroxene, plagio-clase, glass	40.7	49.8

a) Volume percent of melt was determined by a 1000 point mode on metallograph.
b) Weight percent of melt was determined by constrained least squares analysis of phase compositions.
c) Volume percent glass was determined by 850 point mode on metallograph.

This volume percentage of melt, V_m, is given by Equations 1 and 2:

$$V_m \text{ (Ol+Chsp)} = 0.157\ T(°C) - 114.0, \text{ where } T(°C) \geq 1170, \quad 1)$$

$$V_m \text{ (Ol+Chsp+Cpx+Plag)} = 1.36\ T\ (°C) - 1522.7, \text{ where } T\ (°C) \leq 1170. \quad 2)$$

Extrapolation of Equation 1 to $V_m = 100$ corresponds to T = 1360°C for the liquidus. Extrapolation of Equation 2 to $V_m = 0$ yields T = 1119°C for the disappearance of liquid, the solidus temperature.

The measured apparent viscosities of the Kilauea Iki molten basalt between 1250° and 1150°C varied from 30 to 2000 Pa•s. Sigmoidal torque versus rotation speed curves were obtained at all investigated temperatures. The curves are linear at low rotation speeds, less than 0.4 revolutions/second, with a positive slope. This corresponds to Newtonian behavior. However, at higher rotation speeds, the curves are concave toward the rotation speed axis, indicating pseudoplastic behavior. This pseudoplastic behavior becomes more

pronounced at low temperature as the volume per cent of suspended crystals increases. We have analyzed the results in terms of an extended the power law indicated by Equation 3:

$$\log \tau_{yx} = A_1 + A_2\left(\log \left(\frac{du}{dx}\right)\right) + A_3\left(\log \left(\frac{du}{dx}\right)\right)^2 \qquad 3)$$

where τ_{yx} is the stress, and $\left(\frac{du}{dx}\right)$ the strain rate. The apparent viscosity, μ, is given by Equation 4:

$$\mu = \tau_{yx} \Big/ \left(\frac{du}{dx}\right) \qquad 4)$$

Figure 2 is a plot of Equation 3 portraying experimental results obtained at the 1236°C isotherm. Figure 3 is a log-log plot of apparent viscosity as a function of shear rate at the same temperature. The apparent viscosity decreases with increasing shear rate, which is common for pseudoplastic liquids. The log of the viscosity at unit shear rate, log μ_o, is calculated from Equation 3 as log $\mu_o = A_1$.

Log μ_o is plotted as a function of reciprocal temperature in an Arrhenius diagram given in Figure 4. The log viscosity curves illustrated there show a sharp break in slope with decreasing temperature. Data above and below this break have been fitted by limiting straight lines from which apparent activation energies can be calculated. The apparent activation energy in the temperature interval 1250° - 1170°C is 65 + 30 kcal mol^{-1}. For temperatures below 1170°C where appreciable crystallization occurs (see Table 2 and Figure 1) and the system exhibits strongly pseudoplastic behavior, the apparent activation energy is 341 + 42 kcal mol^{-1}. Also shown in Figure 4 are the results of Shaw (3) obtained on a Hawaiian basalt similar to our Kilauea Iki specimen (see Table 1). The general trend of the two sets of data is similar, but the break in the slope of Shaw's data occurs at a lower temperature than it does in ours, presumably because of the change from Newtonian to pseudoplastic behavior in his system. In both studies, the break in the slope of the viscosity curves occurs at 20 to 30 volume percent of suspended crystals. The non-Newtonian behavior of these molten silicate suspensions appears to arise from the increasing volume of suspended crystals in the melt. This suggests that in modeling fluid flow in silicate liquids, power law behavior should be considered when the suspended crystal volume exceeds 20 percent.

REFERENCES

(1) Huebner, J. S. (1971) in Research Techniques for High Pressure and High Temperature, Ulmer, E. C. ed., Springer-Verlag (1971), p. 146.
(2) Shaw, H. R., Wright, T., Peck, D. L. and Okamura, R. (1968) Amer. Jour. Sci., Vol. 266, p. 225-264.
(3) Shaw, H. R. (1969) Jour. Petrology, Vol. 10, p. 510-535.

This work was performed under the auspices of the U. S. Department of Energy by the Lawrence Livermore National Laboratory, under Contract No. W-7405-ENG-48.

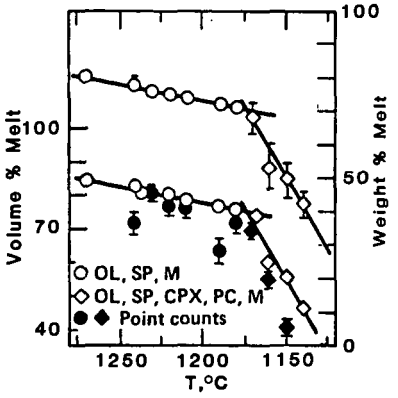

Fig. 1. Volume percent and weight percent melt as a function of temperature for Kilauea Iki basalt. The upper curve gives weight percent melt, indicated by the right ordinate. Open symbols on the lower curve give volume percent melt remaining (left ordinate), calculated from weight percent data and densities of phases. Solid symbols are from modal analyses.

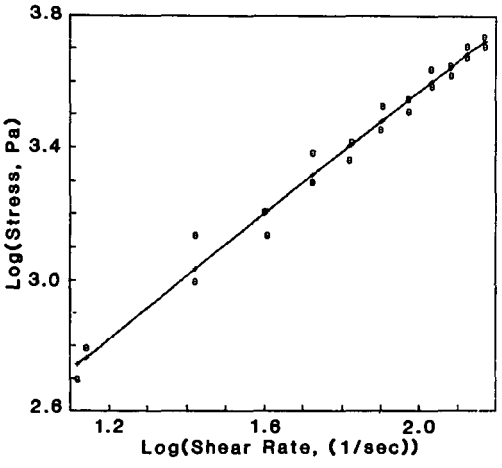

Fig. 2. Log (Stress) as a function of log (Shear Rate) for Kilauea Iki basalt melt at 1236°C.

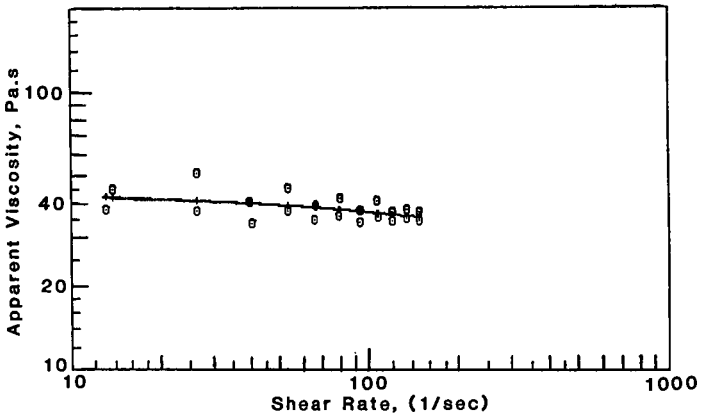

Fig. 3. Apparent viscosity of Kilauea Iki basalt melt as a function of shear rate at 1236°C.

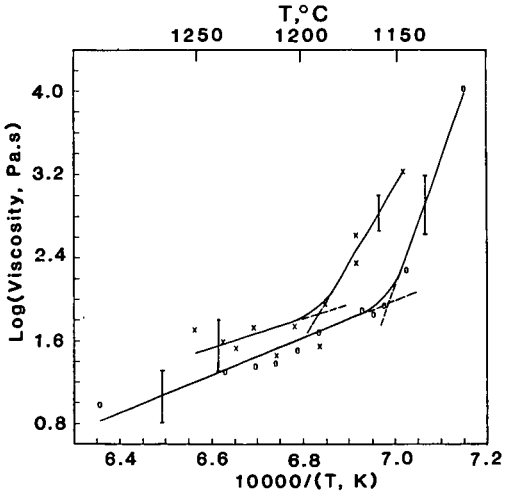

Fig. 4. Log (Apparent Viscosity) as a function of a reciprocal temperature. Present study, X; Shaw (1969), θ.

CRYSTALLISATION OF COAL ASH MELTS

David P. Kalmanovitch and J. Williamson[+]

Energy Research Laboratories, CANMET, 555 Booth St., Ottawa, K1A 0G1, Canada
[+]Department of Metallurgy and Materials Science, Imperial College of Science and Technology, Prince Consort Rd., South Kensington, London, SW7, England.

The formation of ash deposits within p.f. coal-fired boilers may cause severe reduction in heat transfer and thermal efficiency. These deposits vary in nature from friable, slightly sintered fouling to dense, semi-vitreous slags. Utility boiler designers and operators use a variety of methods (9) to ascertain various design criteria or the likelihood of the ash to form deposits (its slagging or fouling propensity). The major technique used is the standard ash fusion test (2) in which a cone or pyramid of coal ash is heated at a given rate, both in air and a mildly reducing atmosphere, while the temperatures at which various degrees of deformation occur are recorded. This method is known to give inaccurate indications of slagging propensity due mainly to the subjective nature of the test and the fact that the technique does not duplicate the thermal history experienced by coal matter in a p.f. boiler.

Various laboratory studies, (5,6) have shown that significant fusion of coal mineral matter, the precursor to ash, occurs within a very short time-frame at temperatures analagous to those in the combustion zone of a boiler (about 1550–1650°C). This is confirmed by microscopical studies of p.f. fly ash. Despite total flight times of about 2s (6) and a temperature gradient ranging from 1650°C to about 300°C the characteristic nature of fly ash, that of hollow cenospheres is due to the presence of significant liquid phase at some stage of the particles' histories. This is further confirmed by mineralogical studies of the particles which sometimes reveals the presence of a refractory phase which had crystallised from a liquid and was not the product of thermal decomposition of an individual coal mineral (4,6). Raask has shown that the growth of deposits is by initial adhesion of fly ash particles to the surface of deposits already present. This adhesion is due to the liquid phase present and the rate of assimilation of the captured particle will be by sintering by viscous flow. From the theory of sintering (6) the rate of increase in strength (s) i.e. growth, of the deposit is given by:

$$\frac{ds}{dt} = \frac{3\gamma k}{2\eta r}$$

Where γ is the surface tension coefficient of the viscous phase, k a constant, r the initial radius of the particles and η the viscosity of the liquid. It can be seen that the nature of a deposit can be described by the degree of sintering which has taken place. For a given coal ash the parameters r and γ are effectively constant with respect to the variability of the viscosity. Therefore the factors which affect the rheological behaviour will determine to a great extent the rate of growth by viscous flow. For homogeneous melts the determining factors are temperature and chemical composition. Lauf has observed that the amount of fly ash particles collected at the outlet of various boilers was inversely proportional to the calculated viscosity (taking account of the different ash contents between the parent coals). (4) The viscosity was calculated by two methods based on the chemical composition; those of Watt and Fereday and Reid. (7,8) The observations confirm the viscosity relation above, albeit qualitatively and the assumption of complete melting of the coal mineral matter. A factor which has not received attention in the literature is the crystallisation of ash particles and/or the deposits already present. With devitrification of a phase from homogeneous melt the composition of the liquid phase will change depending on the precipitating phase and the degree of crystallisation. This in turn will directly affect the viscosity and hence the rate of growth of the deposits.

subjected to a series of crystallisation treatments within the reducing atmosphere. The quenched samples were analysed for phases present by X-ray diffraction and for the ratio of ferrous to ferric iron by a wet chemical technique.

The major observation of the crystallisation study of the ash melts was that the phase or phases which were precipitated contained only the predominant components, the minor components remaining in the liquid phase. Another observation was the reluctance of the melt to crystallise to the expected number of phases; only anorthite ($CaO.Al_2O_3.2SiO_2$) was determined to crystallise for the two western type ashes and mullite ($3Al_2O_3.2SiO_2$) as the primary phase with a secondary phase of iron spinel; a member of the solid solution series magnetite ($FeO.Fe_2O_3$) - hercynite ($FeO.Al_2O_3$), only for the eastern type ash.

The crystallisation of the ternary compositions is discussed with respect to that predicted for each from the phase diagram for the system. The normalized ternary compositions of the two western type ashes were plotted on the phase diagram and the observed crystallisation compared with that predicted from the diagram and the behaviour of the model compositions. The system was found not to be able to correctly predict the primary crystalline phase for one of the two ashes but could account for the crystallisation of anorthite only for the other ash.

As quaternary systems are quite complex both the representation and crystallisation of compositions are discussed in the presentation. Planes of constant MgO content was used as the method of representation of the $CaO-MgO-Al_2O_3-SiO_2$, with planes at 5, 10 and 15 wt% prepared from literature sources and results of this study (3). The observed crystallisation of the glasses studied is discussed in terms of the equilibrium system, a striking observation being the apparent low solubility of magnesia in the compositions studied; a magnesia bearing phase precipitating for nearly all the glasses as primary or secondary phase. The corresponding normalised composition of the western type ashes were plotted on the 5% plane and the observed behaviour compared with the predicted crystallisation behaviour. As with the ternary system the four-component system only correctly predicted the primary crystalline phase for one of the ashes. Also the system would predict that a secondary phase containing magnesia would be expected to crystallise; behaviour which was not observed.

The true representation of the system $CaO-Al_2O_3-SiO_2$-iron oxide is as a quinary system which is too complex for normal analysis. The results of the ferrous to ferric ratio of the quenched samples showed significant amount of ferric iron present. Fortunately analysis of the crystalline phases shows that predominantly the ferrous iron is taken up by the iron bearing phase (there was some evidence of solid solution of ferric iron in the iron spinel phase) and therefore the system could be approximated by the quaternary system $CaO-FeO-Al_2O_3-SiO_2$. Planes of constant FeO content (5-30 wt% at 5% increments) have been prepared from literature sources and the results of the crystallisation studies of the glasses are discussed in terms of the system. Unlike the quaternary system above the iron oxide remains in solution compared with magnesia. This would be predicted from the planes of the system and was observed in the crystallisation studies; no primary phase containing iron oxide was determined even for the glasses containing 20 wt% equivalent FeO. The corresponding normalised composition of the three ashes (iron oxide expressed as equivalent FeO) was plotted on the relevant plane of the system and the observed behaviour compared with that predicted from the phase diagram and the behaviour of the model compositions. The system correctly predicted the primary crystalline phase for all the ashes and could account for the crystallisation of anorthite only for the two western type ashes. While initially the system could not predict the crystallisation of iron spinel as the secondary phase for the eastern type ash analysis of the

Thus it will be of great value to be able to predict to some extent the crystallisation behaviour of coal ash melts. For simplicity it is initially necessary to consider that the crystallisation will be from a homogeneous melt. The data obtained can be extended to the phenomena of boiler deposits by using an accurate model of viscosity of ash melts based on chemical composition. The main aim of the study presented here was to obtain relevant crystallisation data of coal ashes and to model the behaviour so as to be able to predict the devitrification of a given ash. Coal ash is usually described as a mixture of up to 11 oxide components and though various investigators (1) have attempted to simplify the system by using certain equivalences the authors have chosen to use the major three or four components to model the observed behaviour.

For eastern type coal ashes the major components are silica, alumina, iron oxide and lime, whereas for western type ashes the major components are silica, alumina, lime and iron oxide or magnesia. In both cases these may comprise 90 wt% or more of the total composition of the ash. Sanyal and Williamson have shown that the initial crystallisation of two western type ashes of low iron oxide content (5% or less) could be described by the normalised composition on the ternary equilibrium diagram of the system $CaO-Al_2O_3-SiO_2$. The study presented here has extended the investigation to the devitrification of eastern type ash as well as two western type ashes and the crystallisation of model compositions corresponding to the normalised compositions of coal ashes. The systems studied were; $CaO-Al_2O_3-SiO_2$, $CaO-MgO-Al_2O_3-SiO_2$ and $CaO-Al_2O_3-SiO_2$-iron oxide, to ascertain which system or systems govern the behaviour most adequately.

The crystallisation of three coal ashes (two western and one eastern type) was determined under laboratory conditions by fusing a sample in an electric muffle furnace to achieve complete melting of the coal minerals. Devitrification was induced by reducing the temperature to a given level and leaving the sample for a given time. The sample was then quenched, effectively freezing the phases present at the elevated temperatures. The sample was analysed by petrographic microscopy and X-ray diffraction. The treatment was repeated over a range of temperatures and times for each sample.

For the study of the crystallisation of the model compositions five ternary CaO, Al_2O_3 and SiO_2 compositions were chosen which were expected to exhibit different behaviour (from the corresponding phase diagram) while being in the compositional region relevant to coal ashes. Homogenous glasses were produced by fusing the correct mixture of the oxide components. The crystallisation of the glasses was determined in an analagous manner to that used for the ash melts. The same five compositions were used as the basis for the study of the crystallisation of the system $CaO-MgO-Al_2O_3-SiO_2$. Two series of compositions were prepared based on the ternary compositions with 5 and 10 wt% MgO respectively. Glasses were produced and the liquidus and crystallisation behaviour determined by a quenching technique.

As iron oxide exists in two oxidation states (ferrous and ferric) in p.f. ash deposits it was necessary to study the crystallisation of glasses in the system $CaO-Al_2O_3-SiO_2$-iron oxide in a controlled atmosphere; the same as that used in the reducing part of the standard ash fushion test i.e. $CO_2:H_2$ mixture 1:1 v/v. The range of iron oxide content in coal ashes is wider than that of magnesia and hence glasses were prepared with up to 20 wt% equivalent FeO. Two series of glasses were produced based on the five ternary compositions with 5 and 10 wt% equivalent FeO with another two series of glasses based on three of the five composition with 15 and 20 wt% equivalent FeO. The glasses were ground to a fine powder and each was

results of the model compositions indicated that ferric iron present in the liquid phase reduced the solubility of iron oxide which could account for the behaviour.

CONCLUSIONS

Therefore the system $CaO-FeO-Al_2O_3-SiO_2$, governs the initial crystallisation of the ash melts studied. The major aim of this study was to be able to predict the crystallisation of ash melts and relate the behaviour to boiler deposit growth. The phases present in six boiler deposits are compared with that predicted from the corresponding normalised composition in the presentation and shows that for all six (three western and three eastern type) the quaternary system predicts the primary phase. Furthermore the change in composition of the liquid phase for two of the ashes (one slagging the other non-slagging) for a range of degrees of crystallisation shows a great difference in terms of the relative concentration of the components which govern viscosity. While the liquid phase for the non-slagging ash became enriched predominantly in silica (the major viscosity-increasing component) the slagging ash became enriched in viscosity reducing components. This relates directly to the model of deposit growth discussed above and is a confirmation of the model.

The results of the study presented indicate the use of phase equilibria data to be phenomena of p.f. boiler deposits and the possible extension to the prediction of boiler fouling and slagging.

REFERENCES:

1. Barrett, E. P., "The fusion, flow and clinkering of coal ash. A survey of the chemical background." Chemistry of Coal Utilization, Ed. E. Lowry, Vol. 1, 1945, Ch. 15, pp 496-576.

2. British Standard 1016, Pt. 15, 1970. "Methods for the analysis of coal and coke, Fusibility of coal ash and coke ash", pp 14.

3. Kalmanovitch, D. P., "Reactions in coal ash melts", PhD Thesis, Univ. London 1983.

4. Lauf, R. J., "cenospheres in fly ash and conditions favouring their formation". Fuel, 60, 1981, p. 1177-79.

5. Padia, A. S., "The behaviour of ash in pulverised coal under simulated combustion conditions". D.Sc. Thesis, M.I.T., 1976.

6. Raask, E., "Flame imprinted characteristics of ash relevant to boiler slagging, corrosion, and erosion". J. Eng. Power, 104, 1982, p. 858-66.

7. Reid, W. T., method given in "Influence of coal mineral matter on slagging of utility boilers". E.P.R.I. report 736, 1981, p. D-1-4.

8. Watt, J. D. & Fereday, F., "The flow properties of slags formed from the ashes of British coals. Pt. I. Viscosity of homogeneous slags in relation to slag composition". J. Inst. Fuel, 42, 1969, p. 99-103.

9. Winegartner, E. C. "Coal fouling and slagging parameters". A.S.M.E. Special Publication, 1974.

THERMAL CONDUCTIVITY AND HEAT TRANSFER IN COAL SLAGS

K C MILLS

National Physical Laboratory, Teddington, Middlesex, TW11 OLW, UK

1. INTRODUCTION

During the gasification of coal, both molten and solid slags are formed in the converter, and the heat transfer within the gasification chamber is governed to a large extent by the thermal properties of the slag phase. Thus in order to carry out either heat balance or modelling calculations it is necessary to have reliable data for the thermal properties of both solid and liquid coal slags. However, the thermal transfer mechanisms in high temperature processes involving slags are exceedingly complex since heat can be transported by convection, radiation and thermal conduction. The total thermal conductivity (k_{eff}) is, in turn, made up from contributions from (i) the thermal ("phonon") conductivity, k_c, (ii) radiation conductivity, k_R and (iii) electronic conductivity, k_{el}. Heat balance calculations must take account of all these thermal transport mechanisms; consequently it is necessary to study the effects of the various mechanisms for not only do they determine the heat transfer in the gasifier, but they can also critically affect the experimental values derived for the thermal conductivity of the slag. Hence the factors affecting the thermal conductivity of slags will be examined and their effect on the various methods available for the measurement of thermal conductivities will be assessed. Finally, experimental data for the thermal conductivity of slags, glasses and magmas will be evaluated to provide a reliable data base for the thermal conductivity of slags, and to determine the likely effects of variations in chemical composition upon values for coal slags.

2. THERMAL CONDUCTION MECHANISMS

2.1 Thermal "phonon" conductivity (k_c)

Heat is transferred through a medium by phonons, which are quanta of energy associated with each mode of vibration in the sample. This mode of conduction is thus referred to as thermal, phonon or lattice conduction. Scattering of the phonons causes a decrease in the thermal conductivity and hence the conductivity is sensitive to the structure of the sample. Scattering of the phonons can occur by collisions of the phonons with one another, or by impact with grain boundaries or crystal imperfections, such as pores. Thus a low-density, highly-porous material will have a low thermal conductivity. In glassy, non-crystalline materials it has been suggested [1] that thermal conductivity decreases as the disordering of the silicate network increases.

2.2 Radiation conductivity (k_R)

Measurements of the thermal conductivity of glasses were found to be dependent upon the thickness of the specimens used, and this is shown in Figure 1. This behaviour was ascribed to the contribution from radiation conductivity, k_R, which can occur in semi-transparent media like slags and glasses. Radiation conductivity occurs by a mechanism involving absorption and emittance of radiant energy by various sections through the medium. Consider a thin section in the slag, radiant energy absorbed by the section will cause it to increase in temperature and consequently radiant heat will be emitted to cooler sections. This process can occur right through the medium and it is obvious that the energy transferred in this way will increase with increasing number of sections (ie increasing thickness) until the point where k_R attains a constant value. At this point the slag is said to be "optically thick", and this is usually considered to occur when $\alpha d > 3.5$, where α and d are the absorption coefficient and thickness of the slag, respectively.

At high temperatures, radiation conductivity can be the predominant mode of conduction, eg in glassmaking more than 90% of the total conductivity occurs by radiation conduction. The radiation conductivity can be calculated for an optically-thick sample if steady-state conditions apply and if it is assumed that the absorption coefficient of the medium, α, is independent of wavelength, λ, ie grey-body conditions obtain. For these conditions k_R can be calculated by use of equation 1), where σ and n are the Stefan-Boltzmann constant and refractive index, respectively.

$$k_R = \frac{16\sigma n^2 T^3}{3\alpha} \quad . \qquad 1)$$

Values of k_R cannot be calculated for optically-thin samples ($\alpha d < 3.5$) and for some measurement techniques involving non-steady state conditions. Thus it is obvious that reliable values of thermal conductivity can only be obtained when either k_R is negligible, or where it can be calculated reliably for optically-thick conditions.

Absorption coefficient (α)

The absorption coefficient is a very important parameter, as it determines (i) the magnitude of k_R (equation 1) and (ii) the thickness at which a slag becomes optically thick ($\alpha d > 3.5$). Hence increasing α has the effect of decreasing k_R and decreasing the depth at which a slag becomes optically thick. If a particular slag sample were optically thin, these two factors would operate in opposition to one another.

The absorption coefficient is markedly dependent upon the amounts of FeO and MnO present in the slag [2]; although Fe_2O_3 absorbs infra-red radiation, its effect on α is much less pronounced than that of FeO. An empirical rule has been derived[2] for glasses containing less than 5% FeO, the absorption coefficient at room temperature is given by the relationship, $\alpha = 11.$ (% FeO).

A basic assumption adopted in deriving equation 1) was that α was independent of wavelength; however, in practice the spectral absorption coefficient (α_λ) varies with the wavelength (λ) as shown in Figure 2 for a glass containing ca. 5% FeO[3]. It can be seen from this figure that there is strong absorption by FeO at ca. 1 μm and by SiO_2 at ca. 4.4 μm. At high temperatures this restricts absorption by the slag to a "window", in the wavelength range 1-4.4 μm. However, even within this wavelength band there is some variation in α_λ and the average absorption coefficient, α_m, is determined by weighting of the α_λ values.

The average absorption coefficient, α_m, can be affected by temperature in two different ways. Firstly, the absorption spectrum, ie, (α_λ), can change markedly with temperature and consequently alter the value of α_m. Secondly, even if the absorption spectrum is unaffected by temperature, α_m would continue to be a function of temperature because the wavelength distribution used in deriving α_m is itself a function of temperature. This can be seen in Figure 3 where the fraction of total energy emitted in the "window" 1-4.4 μm constitutes 61.1%, 79.5% and 81.9% of the total energy emitted at 1073K, 1573K and 1773K, respectively. In a similar manner, the various α_λ values of the spectrum will have to be weighted differently in the calculation of α_m for the three temperatures in question.

It can be seen from Figure 2 that α_m increases with increasing temperature, and similar behaviour has been observed in rocks and minerals [4,5,6]. By contrast, the absorption coefficients (α_m) of amber glass have been found to decrease with increasing temperature.

Extinction coefficient (E)

In solids, radiant energy can be scattered by grain boundaries, pores and cracks in the material. In these cases, it is necessary to use the extinction coefficient (E) which is given by the relationship $E = \alpha + s$, where s is the scattering coefficient.

2.3 Electronic conductivity (k_{el})

It has been reported that glasses which contain significant concentrations of Fe^{2+} ions behave in a similar manner to semi-conductors and hence thermal conduction via conduction electrons, holes, etc. could be significant, according to Fine et al[7]. Little is known of this mechanism in relation to the heat transfer in slags and consequently the contribution of k_{el} to the measured thermal conductivities has been ignored in this review.

2.4 Total thermal conductivity (k_{eff})

In practice, the radiation and conduction contributions to the heat flux (Q) are interactive, and the interpretation of the combined conductive-radiative heat transfer is exceedingly complex. Various models have therefore been proposed to simplify the theory of the heat transfer process. One widely-used model is the diffusion approximation which assumes that the heat flux (Q) is given by equation 2), where k_{eff} is the effective thermal conductivity and is defined by equation 3) where x is the distance. Gardon [8] has pointed out that this model only applies strictly when (i) k_R is small and (ii) $\alpha d > 8$.

$$Q = -k_{eff} (dT/dx) \quad 2)$$

$$k_{eff} = k_c + k_R \quad 3)$$

3. EXPERIMENTAL METHODS FOR DETERMINING THERMAL CONDUCTIVITY

The experimental methods available for measuring thermal conductivities are summarised below; more detailed reviews of the experimental techniques are available elsewhere [3,9,10,11]. The techniques can be divided into three classes: (i) steady-state methods, (ii) non-steady state methods, and (iii) indirect methods for the determination of k_R. The steady-state methods usually yield k_{eff} values and the non-steady state techniques usually produce thermal diffusivity (a_{eff}) values, which can be converted to thermal conductivity values by use of equation 4), where ρ and Cp are the density and heat capacity of the slag.

$$k = a . Cp . \rho \quad 4)$$

3.1 Steady-state methods

These methods all yield k_{eff} values provided that the specimen is optically thick.

In the linear heat-flow method two disc-shaped specimens are placed on either side of an electrically-heated plate and the temperature profiles across the samples are monitored by thermocouples sited on both faces of the specimens. The apparatus is well insulated to minimise heat losses. In some versions of this method, the total heat fluxes passing through the samples are determined by calorimeters in contact with the specimens. When high-temperature measurements are required, this technique is usually operated as a comparative method [12].

In the radial heat-flow method the specimen is in the shape of a hollow cylinder, which is sited in the annulus between two coaxial cylinders with the internal cylinder acting as a radial heat source [13]. The temperature profile across the specimen is determined by thermocouples placed on the inside walls of the two cylinders. This method requires a large isothermal zone in the furnace, which is difficult to achieve at high temperatures. When this technique is used for measurements on liquids it is prone to errors from convective heat transfer.

3.2 Non-steady state methods

In the radial wave method the slag is placed in a cylindrical crucible sited in the isothermal zone of a furnace, and thermocouples are located on the walls and along the geometric axis of the crucible (the slag). The outside wall of the

of the crucible is then subjected to a sinusoidal variation of temperature and the variation in temperature of the central thermocouple is monitored. There is a phase shift between the input and output which is related to the thermal diffusivity of the slag. In the modification of this apparatus used by Elliott and co-workers[7,14] the periodic variation in temperature is produced in a wire running along the central axis of the cylindrical crucible, and the phase shift is measured in the signal of the thermocouples sited on the walls of the crucible. The thermal diffusivity values obtained with this method may be vulnerable to errors arising from convective heat transfer.

In the modulated beam method the specimen is in the form of a disc, which is maintained at a constant temperature, whilst the front face of the disc is subjected to a laser beam which produces a periodic variation in temperature of constant frequency. The phase shift between this input and the signal from a temperature sensor in contact with the back face is determined. By carrying out measurements at two or more frequencies, Schatz and Simmons[6] were able to derive values of both a_{eff} and the extinction coefficient. If this method were applied to measurements in liquids, it too would be prone to errors caused by convection.

The laser pulse method[15,16] when applied to solids uses a disc-shaped slag specimen coated with metallic films on both planar surfaces. A laser pulse is directed on to the front face of the specimen and the temperature of the back face is monitored continuously. The maximum temperature rise of the back face (ΔT_{max}) usually occurs after ca. 10 seconds, and a_{eff} may be computed from the time taken ($t_{0.5}$) for the back face to attain a temperature rise of ($0.5\ \Delta T_{max}$). The method has also been applied to measurements on liquid slags[15,17] which were contained in Al_2O_3 or BN crucibles. The major advantage of this technique is that the short duration of the experiment minimises the errors due to convection. The major disadvantage is that the maximum specimen thickness is about 4 mm, and consequently optically-thick conditions only apply when the extinction coefficient is greater than 9 cm^{-1}. A second disadvantage is that the laser pulse method is a transient technique and k_R cannot be calculated by equation 1), which is applicable to steady-state conditions; at the present time no formulae exist for the calculation of k_R for this method. Thus this technique is most useful when applied to specimens which have (i) very small values of αd (ie $\alpha d \ll 3.5$) where $a_{eff} \simeq a_c$, or (ii) large extinction coefficients where k_R is negligible and thus $a_{eff} = a_c$.

The line source method is also a transient technique and is the standard method for measuring the thermal conductivities of liquids at lower temperatures. In the high-temperature versions, this method consists of a fine Pt wire (ca. 0.1 mm dia) which is sited centrally in a crucible of molten slag. This wire acts as both heating element and temperature sensor. When an AC or DC current is applied to the wire, the temperature rise of the wire (ΔT) is monitored continuously during the heating period (ca. 1 second). A linear relationship exists between ΔT and ln (time), the slope of which is proportional to (1/k). This method has the advantage that convectional heat transfer is eliminated (if convection does occur it results in a non-linear ΔT-ln (time) plot and can therefore be readily detected). Routines are available for calculating the value of k_R for optically-thick conditions[18]; however, de Castro et al.[19] have recently proposed that k_R is negligible in the values of k_{eff} measured by this technique at ambient temperatures (ie $k_R \simeq 0$, $k_{eff} = k_c$). There is evidence to support the view that $k_R \simeq 0$, as measurements made with this technique at higher temperatures[20,21,22] yield much lower values of k_{eff} for slags than those obtained by steady-state techniques. Furthermore, Powell and Mills[23] have pointed out that the thermal conductivity data for molten salts become more consistent if k_R is taken to be zero in the various line-source determinations.

3.3 Indirect measurements of k_R

The absorption (or extinction) coefficient can be determined by measurement of the optical transmissivity (τ) of the slag as a function of wavelength; the absorption coefficient (α) is given by equation 5), where d is the thickness of the specimen.

Measurements at high temperatures are carried out by using

$$\alpha_\lambda = -\ln(\tau_\lambda)/d \qquad 5)$$

an assembly of mirrors to direct a beam of radiation of known frequency on to a disc-shaped specimen sited in a tube furnace. The transmitted beam is diverted into an infrared spectrophotometer where the transmissivity is determined. Blazek and Endrys[3] have reported that k_R values for glasses calculated from absorption coefficient data are in good agreement with values of $(k_{eff} - k_c)$ determined experimentally.

3.4 Summary of experimental limitations

(i) It is important to ensure that the thermal conductivity measurements on semi-transparent media should be carried out with optically-thick specimens, as k_R cannot be calculated for optically-thin conditions. It is recommended that absorption coefficient measurements should also be carried out to determine the slag thickness required to produce an optically-thick specimen.

(ii) The non-transient techniques are prone to errors due to convectional heat transfer.

(iii) At the present time no reliable routines are available for calculating the k_R contribution to the overall thermal conductivity measured in transient techniques; there is some evidence to suggest that k_R is negligible in measurements obtained by the line source method.

4. REVIEW OF THE EXTANT DATA FOR SLAGS

There is a paucity of data for coal slags; it is therefore necessary to study a much broader range of slags in order to determine the effects of compositional change on the thermal conductivity of the slag. One problem continually encountered is that the distribution of Fe in slags between (Fe^{3+}), (Fe^{2+}) and free iron is not reported, and this can have a marked effect on the absorption coefficient and consequently k_R. Furthermore, the ratio of $((Fe^{2+})/(Fe^{3+}))$ is known to vary with (i) temperature, (ii) $p(O_2)$ and (iii) the composition of the slag, (Fe^{2+}) increasing with increasing SiO_2 and TiO_2, and decreasing CaO and Na_2O.

4.1 CaO + SiO_2 + FeOx

Fine et al[7] determined the absorption spectra at room temperature of three slags containing 0, 7 and 14% FeO (Figure 4). The absorption coefficients of the slags containing 7 and 14% FeO will probably increase with increasing temperature as the (Fe^{2+}/Fe^{3+}) ratio increases with increasing temperature. An increase in α with increasing temperature can also be seen in Figure 2. Fine et al[7] used the radial wave method to determine a_{eff} of solid and liquid slags containing 0 to 25% FeO; their results are summarised in equation 6), where B represents the basicity, ie (CaO/SiO_2) ratio and T is the temperature in (°C).

$$a_{eff} = 10^{-7}\,(1.5 - 0.5\,B) + 1.8 \times 10^{-6}\,\frac{(T/1500)^3}{(\%FeO)^{0.8}}\ m^2 s^{-1} \qquad 6)$$

This equation indicates that increasing the FeO content results in a reduction of a_{eff}; this behaviour is due presumably to the increase in α and hence the consequent decrease in k_R with increasing FeO content. However, Nauman et al[24] using the same experimental technique as Fine et al[7] obtained the k_{eff} - (% FeO) relationship shown in Figure 5 for molten slags with high FeO contents. The density of slags are known to increase with increasing (FeO_x, MnO) content, thus $k(= a.C_p.\rho)$ would be expected to increase as the level of FeO increases[25]. However, calculations have shown that this increase in k would be ca. 30%, and this alone would not account for the increase in k shown in Figure 5. Thus it must be concluded that FeO additions do increase the thermal diffusivity of the

system. In these slags with high FeO content, the absorption coefficient must be very high and thus k_R must be negligible and $k_{eff} = k_c$.

4.2 $CaO + Al_2O_3 + SiO_2$

Measurements on solid slags have been reported by Kingery[12] (comparative linear heat-flow method), Osinovskikh[25] and Susa et al[21] (line source method), and for the liquid phase by Susa et al[21] and Ogino et al[13] (radial heat-flow); the results are summarised in Figure 6. The data recorded by Osinovskikh[25] appear to be too low, but there is some measure of agreement between the data obtained for the liquid near the liquidus temperature (T_{liq}). However, the reported, thermal conductivity values diverge as the temperature increases, and this is possibly due to the negligible contribution of k_R in the line source measurements[20] and the effects of k_R and convective heat transfer on the value due to Ogino[13]. The value due to Kingery[12] for the compound $3Al_2O_3.SiO_2$ is appreciably higher than that for the slags of the ternary system.

4.3 $MgO + Al_2O_3 + SiO_2$

Values for the various binary compounds occurring in this system have been reported by Rudkin[26] and by Kingery[12] (comparative linear heat-flow method), and by Schatz and Simmons[6] (modulated beam method) for temperatures up to 1300 °C; there is excellent agreement between the values due to the latter two groups of workers. Schatz and Simmons[6] reported that extinction coefficient of $2MgO.SiO_2$ increases from 5 cm^{-1} at 270 °C to 25 cm^{-1} at 1300 °C.

4.4 $Na_2O + SiO_2$

Susa et al[21] (line source method) reported thermal conductivity data for solid and liquid slags for three compositons; the single value obtained by Ogino et al[13] (radial heat-flow method) is in reasonable agreement with these data.

4.5 Glasses

Blazek and Endrys[3] have reviewed the thermal conductivity data for glasses. The lattice thermal conductivity, k_c, for glasses is relatively unaffected by composition and was found to increase with temperature from 1 $Wm^{-1}K^{-1}$ at 25 °C to 2.7 $Wm^{-1}K^{-1}$ at 1300 °C. However, the radiation conduction is frequently the dominant mode of heat conduction in glasses at high temperatures.

4.6 CaF_2-based slags

Extinction coefficients have been reported (1.3 cm^{-1} for 1000-1300 °C) by Keene and Mills[27], and absorption coefficients (1.3 cm^{-1}) for the liquid state by Mitchell and Wadier[22].

The thermal conductivity values for polycrystalline (optically-thick) CaF_2 obtained by Kingery[12] (comparative linear flow method) and by Taylor and Mills[16] are in reasonable agreement (Figure 7). However, there is an appreciable discrepancy between the values of k obtained by the line source method[20-22] and the single value due to Ogino et al[13] (radial heat source method).

The reason for the discrepancy probably lies in the magnitude of the k_R values measured in the two experiments, as k_R is probably negligible for the line source technique, in contrast to the steady-state method where k_R would be appreciable despite the fact that the sample was probably optically thin ($\alpha d \simeq 0.8$).

4.7 TiO_2-based slags

Values of thermal diffusivity, a_{eff}, of ca. 3×10^{-7} m^2s^{-1} have been reported by Raflovich and Denisova[28] for slags based on TiO_2 (>45%) and SiO_2 with small

amounts of Al_2O_3 and Fe_2O_3. The data reported by Osinoskikh et al[25] for slags with less than 15% TiO_2 are much lower, this is probably due to the high porosity of the sample used.

4.8 Continuous casting slags

These slags have the approximate composition (CaO = SiO_2 = 35%; Al_2O_3 ≈ 7%; Na_2O (4-15%) and CaF_2 (5-8%). Olusanya[29] has reported that the absorption coefficients lie in the range (0.5 - 5 cm^{-1}) and thus k_R could be appreciable in these slags. Values for a_{eff} were obtained for ten glassy-slags by Taylor and Mills[30] (laser pulse method) which lay between 4 and 5 x 10^{-7} m^2s^{-1} (Figure 8); these slags were optically thin (αd = 0.4) and thus we might expect k_R to be small and $k_{eff} \simeq k_c$. Some crystallisation of the samples occurred at temperatures above the glass temperature in these experiments, and this resulted in an initial decrease in a_{eff}, which was subsequently followed by an increase in the thermal diffusivity. Taylor and Mills reported that a_{eff} of a crystallised specimen had a value of 6 x 10^{-7} m^2s^{-1}, which is higher than that of the glassy specimens; the crystalline samples would have a higher extinction coefficient and thus k_R would be low and hence $a_{eff} = a_c$. Thermal conductivity values for the liquid phase have been obtained by Nagata et al[31] and by Powell et al[32] (line source method), and by Taylor and Edwards[17] (laser pulse method) and by Ohmiya et al (33) interpretation of thermal flux data). As can be seen from Figure 8, the results from the line source technique are lower than the other data, and this probably reflects the fact that k_R is negligible in the line source experiements. The increase in k_{eff} observed by Taylor and Edwards[17] above the solidus temperature is probably due to the decrease in α (and increase in k_R), as liquid is formed from crystallised slag.

4.9 Blast furnce slags

Values of k_{eff} have been reported by Ischenko[34] and by Vargaftik and Oleschuk[35] for temperatures in the range (200-1000 °C). The values cited are lower than those reported for other slags, which is presumably due to the high porosity of the samples used by these workers.

4.10 Rocks and Minerals

Absorption and extinction coefficients for several rocks and minerals[4,5,6] were found to increase appreciably at high temperatures, eg α_M (peridot) increases from 0.5 cm^{-1} at 25 °C to 4.3 cm^{-1} at 1240°C. Values of k_{eff} (or a_{eff}) have been recorded by Kingery[12], by Kawada[36] (comparative linear flow method), by Murase and McBirney[37] (radial heat flow), and Schatz and Simmons[6] (modulated beam method). The results are given in Figure 9, and Schatz and Simmons[6] reported that for forsterite and olivine at 1300 °C, approximately half of the measured k_{eff} value was due to the contribution of k_R. There is good agreement between the results reported by Kingery[12] and by Schatz and Simmons[6] for k_{eff} of forsterite. The values of k_{eff} reported by Murase and McBirney[37] are appreciably lower than those reported by other investigators, which may indicate systematic errors in the method, or may merely be due to the higher SiO_2 content of the samples studied by Murase and McBirney. The sharp increase in k recorded above 1100 °C for some samples probably indicates the onset of melting, which causes the extinction coefficient to decrease and hence k_R to increase appreciably. It is noticeable that Kawada[36] recorded no marked increase in k_{eff} for dunite (DU), which has an FeO content of 13% and where k_R would be negligible.

4.11 Coal slags

The experimental details of various investigations concerned with these slags are summarised in Table 1. The results are presented in Figure 10; only the upper and lower a-(T) curves reported by Gibby and Bates have been plotted.

The absorption coefficients of these slags are probably quite high, as they contain appreciable levels of FeO and free Fe. Thus the radiation contribution, k_R, will

be relatively small. There is good agreement between the results of the investigations when the appreciable differences in the composition of the slags is taken into account. Gibby and Bates[15] reported that for solid slags the value of a_{eff} varied appreciably from run to run and appeared to be dependent upon the thermal history of the sample. This behaviour was attributed to the crystallinity of the sample and the fact that a_{eff} (crystalline) $>$ a(glass), which is in agreement with the observations on continuous-casting slags. Gibby and Bates[15] also observed that K_2O additions resulted in a decrease in a_{eff} up to 900 °C, and that the a_{eff}-(T) relationship showed a sharp inflection around 950 °C, which was attributed to the crystallisation of the slags.

These workers also reported that a_{eff} appeared to decrease with increasing SiO_2 content or with the ratio $(SiO_2/(SiO_2 + Fe_2O_3 + MgO + CaO))$. This implies that k_c is probably dependent upon the structure of the silicate slag, and thus it should be possible to build up a reliable model for the estimation of k_c in due course. However, it is also possible that the decrease in a_{eff} with increasing SiO_2 content may simply reflect the lower fraction of crystalline phase present in the slag.

5. DISCUSSION

The thermal conductivity data for slags, magmas and glasses have been collated in Figure 11. It can be seen that k_{eff} values for solid coal slags are similar to those for slags from the systems $CaO + Al_2O_3 + SiO_2$ and $CaO + SiO_2 + FeO$ and for those used in continuous casting. Thus it would appear that the chemical composition of the slag has little effect on the values of k_{eff}; however, certain oxides (eg SiO_2, CaO) could exert some influence on the conductivity by altering the crystallinity of the slag. Furthermore, the radiation conduction will also be affected by the crystallinity of the sample as the extinction coefficient will be high for crystalline materials.

It is more difficult to evaluate the thermal conductivity of molten slags, although the data obtained for coal slags[15] and for slags of the system $CaO + FeO + SiO_2$ [7][14] indicate that k_{eff} for the liquid near the melting-point is similar to that for the solid phase . It is noticeable that the k_{eff} values obtained for liquid slags by the line source method are considerably lower than the values obtained with other techniques. It is possible that the line source method is prone to systematic errors when applied to molten slags, but a more likely explanation is that the k_R is negligible in these experiments. As coal slags contain relatively high levels of $(FeO + Fe_2O_3)$, it would be expected that the absorption coefficient of the slag would be high and that the k_R contribution would be small. However k_R increases dramatically with temperature and even a slag with a relatively high absorption coefficient of 100 cm^{-1} would give rise to a contribution of k_R of 0.4 $Wm^{-1}K^{-1}$ at 1800 K.

However as the absorption coefficient is very dependent upon the (Fe^{2+}) concentration the value of k_R will be dependent upon the various factors affecting the (Fe^{2+}/Fe^{3+}) ratio in the slag viz. the ratio increases with (i) increasing temperature (ii) decreasing p (O_2) (iii) increasing SiO_2 and TiO_2 contents and decreasing CaO, Na_2O and K_2O contents in the slag. This review has revealed the urgent need for absorption coefficient data for coal slags at high temperatures and for information relating the absorption coefficient to the FeO content of the slag.

The heat transfer process in the coal gasifier can also be affected by the layer of slag which lines the walls of the gasifier. Recently, Grieveson and Bagha [38] have developed a simple experiment for measuring the thermal flux (Q) in various slags used in the continuous casting of steel. A water-cooled, copper finger is lowered into a crucible containing molten iron covered with a layer of slag and a layer of solidfied slag forms around the cold finger. The thermal flux is determined by measuring the

temperature rise of the cooling water flowing through the copper finger. It was found that the heat flux was related to (i) the thickness of the slag layer and (ii) the thermal resistance of the Cu/slag interface. The thickness of the slag layer is, in turn, dependent upon the viscosity of the slag and upon other factors determining the "melt back" of the slag layer. Grieveson and Bagha [38] observed that the thermal resistance of the Cu/slag interface appeared to be related to (i) the mineralogical constitution of the slag and (ii) the strength of the adhesion between the copper and the slag eg. Q (glass from $CaO.SiO_2$ field giving good Cu/slag adhesion) > Q (glass from $CaO.Al_2O_3.2SiO_2$ phase field with poor Cu/slag adhesion). Thus relatively simple experiments like these simulation tests can provide us with a valuable insight into the factors affecting heat transfer mechanisms occurring in industrial processes.

CONCLUSIONS

(i) Experimental data for the thermal conductivities of slags must be carefully analysed to establish the boundary conditions of the experiment (eg. optical thickness of the specimen, magnitude of k_R etc.) This evaluation of the data allows one to determine the suitability of a specific thermal conductivity value for subsequent use in heat balance calculations for the gasifier.

(ii) The thermal conductivities of coal slags are not very dependent upon the chemical composition of the slag.

(iii) The thermal conductivity of a slag is dependent upon the degree of crystallization and consequently upon the thermal history of the specimen; the thermal conductivity of the crystalline phase is greater than that of the glassy phase.

(iv) The radiation conduction, k_R, is principally determined by the magnitude of the absorption (or extinction) coefficient. As the absorption coefficient of the slag is largely dependent upon the (Fe^{2+}) concentration in the slag, it will also be dependent upon the factors affecting the (Fe^{2+}/Fe^{3+}) ratio viz. temperature, $p(O_2)$ and the SiO_2, CaO and Na_2O contents of the slag.

(v) Experimental data are required for the absorption coefficients of coal slags at high temperatures so that the relationship between α_m and the FeO content can be established.

(vi) Heat transfer in the coal gasifier will be partially dependent upon the thermal resistance of the slag/wall interface and this, in turn, will be dependent upon the mineralogical constitution of the slag adjacent to the wall.

ACKNOWLEDGEMENTS

Valuable discussions with B J Keene, (National Physical Laboratory) Professor P Grieveson (Imperial College) and Dr R Taylor (UMIST) are gratefully acknowledged.

REFERENCES

(1) AMMAR, M M., GHARIB, S, HALAWA, M M, E L BADRY, K, GHONEIM, N A and E L BATAL, H A. J. Non-Cryst. Solids 1982, 53, 165.

(2) STEELE, F N and DOUGLAS, R W. Phys. Chem. Glasses 1965, 6, 246.

(3) BLAZEK, A and ENDRYS, J. Review of thermal conductivity data in glass, Part II Thermal conductivity at high temperatures published Intl. Commission on Glass, 1983.

(4) FUKAO, Y., MITZUTANI, H. and UYEDA, S. Phys. Earth Planet Interiors 1968, 1, 57.

(5) ARONSON, J R, BELLOTI, L H ., ECROAD, S W, EMSLIE, A G., MCCONNEL, R K and THUNA, P C von. J Geophys. Res. 1970, 75, 3443.

(6) SCHATZ, J F and SIMMONS, G. J. Geophys. Res. 1972, 77, 6966.

(7) FINE, H A; ENGH, T, and ELLIOTT, J H; Metall. Trans B, 1976, 7B, 277.

(8) GARDON, R; paper presented at 2nd Intl. Thermal Conductivity Conference, Ottawa, 1962, 167.

(9) GARDON, R Review of thermal conductivity data in glass, Part 1 Thermal conductivity at low and moderate temperatures published Intl. Commission on Glass, 1983.

(10) TOULOUKIAN, Y S , POWELL, R W, H O, C Y and KLEMENS, P G. Thermophysical Properties of Matter, volumes 1 (1970) and volume 10 (1973) published by IFI/Plenum, New York

(11) TYE, R P, Thermal conductivity, volumes 1 and 2, 1969, published by Academic Press, New York.

(12) KINGERY, W D, FRANCL, J, COBLE, R L and VASILOS, T. J. Amer. Ceram. Soc., 1954, 37, 107.

(13) OGINO, K, NISHIWAKI, A, YAMAMOTO, K and HAMA, S. Paper presented at Intl. Symp. Phys. Chem. Steelmaking, Toronto, 1982, III-33.

(14) NAUMAN, J; FOO, G; and ELLIOTT, J F; Extractive Metallurgy of Copper, Chapter 12, 237.

(15) GIBBY, R L and BATES, J L; 10th Thermal Conductivity Conference, held Newton, Mass., Sept. 1970, IV-7,8. see also BATES, J L, Final Report to National Science Foundation, Grant GI-44100 Properties of Molten coal slags relating to open cycle MHD, Dec. 1975.

(16) TAYLOR, R and MILLS, K C; Arch. f. Eisenhuttenw., 1982, 53, 55.

(17) TAYLOR, R and EDWARDS, R. cited by MILLS, K C and GRIEVESON, P, a paper presented at the Centenary Conference 1984, "Perspectives in Metallurgy" Sheffield University,July 1984.

(18) SAITO, A; Bull. Jap. Soc. Mech. Engr., 1980, 23, 1459.

(19) de CASTRO, C.A.N, L I, S.F.Y., MAITLAND, G.C. and WAKEHAM, W.A, in press Intl. J Thermophys. (1984)

(20) MILLS, K C; POWELL, J S; BRYANT, J W and KEENE, B J, Canad, Metall. Q, 1981, 20, 93.

(21) SUSA, M, NAGATA, K and GOTO, K S; Trans, Iron Steel Inst. Japan, 1982 22 B42.

(22) MITCHELL, A and WADIER, J F; Canad. Metall. Q, 1981, 20, 373.

(23) POWELL, J S, and MILLS, K C. Paper to be presented at the Ninth European Conference on Thermophysical Properties to be held in Manchester, Sept. 1984.

(24) MILLS, K C. Paper entitled "Estimation of physico-chemical properties of coal slags and ashes" to be presented at this conference.

(25) OSINOVSKIKH, L L, KOCHETOV, N N and BRATCHIKOV, S G; Trudy Urals N-I Chern. Met., 1968 (8), 71.

(26) RUDKIN, R L; Report US AF., ASD-TDR-62-24 II.

(27) KEENE, B J and MILLS, K C. Arch f Eisenhuttenw. 1981, 52, 311.

(28) RAFALOVICH, I M and DENISOVA, I A; Fiz. Khim Rasplav. Schlakov, 1970, 181.

(29) OLUSANYA, A, "The Fundamental Properties of Continuous Casting Fluxes" PhD Thesis, Imperial College, London, 1983.

(30) TAYLOR, R, GRIEVESON, P, TAYLOR, R. Paper entitled "Thermal and Physico-chemical properties of continuous-casting slags" to be presented at Ninth European Conference on Thermophysical Properties to be held in Manchester Sept. 1984.

(31) NAGATA, K and GOTO, K S. private communication, Tokyo Inst. of Technology, 1984.

(32) POWELL, J. S., MILLS, K C unpublished thermal conductivity data on casting powders, National Physical Laboratory, 1984.

(33) OHMIYA, S; TACKE, K H and SCHWERDTFEGER, K; Ironmaking and Steelmaking, 1983, 10, 24.

(34) VARGAFTIK, N B and OLESHCHUK, O N; Teploenergetika, 1955, 4, 13.

(35) ISCHENKO, K D; Met. Kobosokhim, 1970, (21) 82.

(36) KAWADA, K; Bull. Earthquake Res. Inst., 1966, 44, 1071.

(37) MURASE, T. and McBIRNEY, A R; Science, 1970, 170, 165.

(38) GRIEVESON, P and BAGHA, S cited by MILLS, K C and GRIEVESON, P in a paper presented at the Centenary Conference 1984, "Perspectives in Metallurgy", Sheffield University, July 1984

Table I

Reference	No	Slag composition					Sample	Method	Temperature Range °C
		%CaO + MgO	%SiO_2	%FeO	%Fe_2O_3	%Al_2O_3			
Vargaftik[34]	A	12.8	35.9	29.0	5.3	14.3	Liquid, solidfied slag; (10 mm) *softening point* ~ ca. 1000 °C	Radial heat flow method. Pt and stainless steel crucibles	25 - 1348
	B	3.8	53.5	14.1	6.0	22.7			25 - 1283
	C	2.2	50.8	21.0	-	13.0			25 - 1151
Gibby and Bates[15]			33-61	6-9	6-36	14-32	6 samples, liquid and solid	Laser pulse method	100 - 1600
Taylor[30]		27	34	6.5	4.5% free Fe	22 +3% Na_2O	Glass, (1 mm)	Laser pulse method	200 - 950

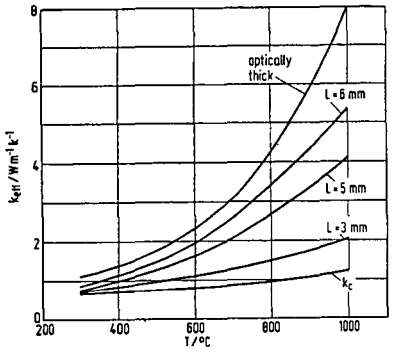

Figure 1. The dependence of k_{eff} upon the thickness of the sample.

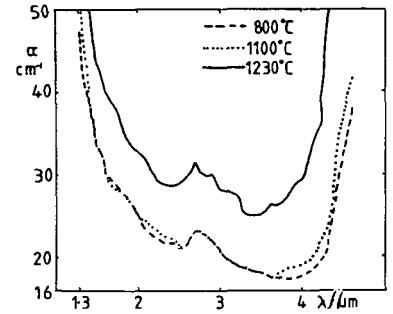

Figure 2. The wavelength of dependence of a glass containing 67 % SiO_2, 16 % Na_2O + 9.% (FeO + Fe_2O_3)

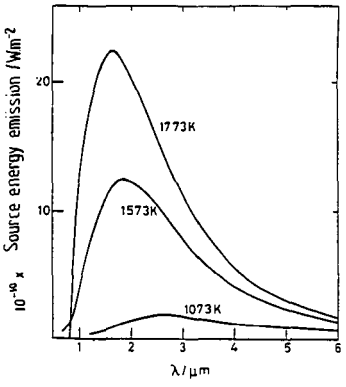

Figure 3. Wavelength distribution of the source energy emission for a black body.

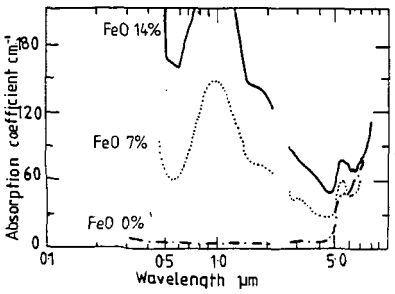

Figure 4. The absorption spectra at room temperature for slags containing FeO_x + CaO + SiO_2.

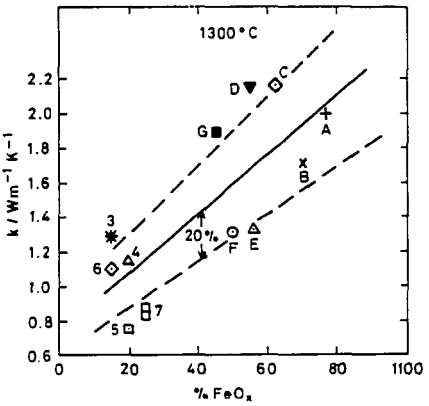

Figure 5. The thermal conductivity of slags of the system FeO_x + CaO + SiO_2 as a function of the FeO_x content. The letters and numerals refer to the specimen numbers (14).

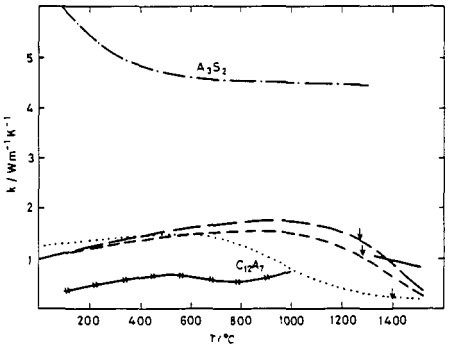

Figure 6. Thermal conductivities of slags from the system, CaO + Al_2O_3 + SiO_2, ——.——.——, Kingery for $3Al_2O_3.2SiO_2$; ———, Ogino et al ; Susa et al, ..., 50% CaO + 50% Al_2O_3; — — — — —, 40% CaO + 40% SiO_2 + 20% Al_2O_3; ——— ———, 25% CaO + 60% SiO_2 + 15% Al_2O_3; —||—, Osinovskikh; ▼, T_{liq}.

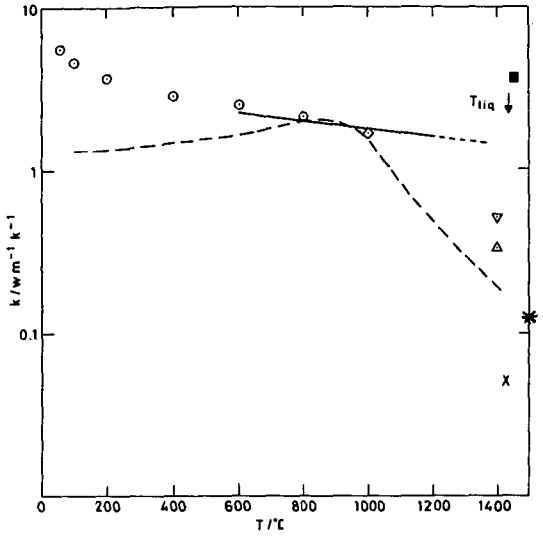

Figure 7. The thermal conductivity of CaF_2 and CaF_2- based slags; CaF_2; *, Powell; ⊙, Charvat; ——— - - -, Taylor; x, Nagata; ■, Ogino; ▽, Mitchell; CaF_2-based slags, — — — —, Susa et al; △, Mitchell.

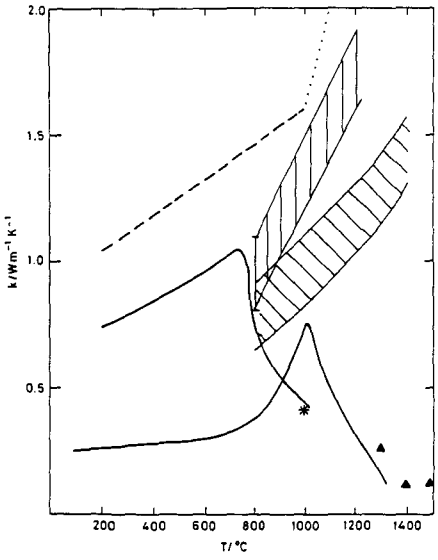

Figure 8. Thermal conductivity of continuous-casting slags; — — — —; •••• Taylor, and Taylor and Edwards; ——, Nagata; ▥, Ohmiya; *, average k_c value, Ohmiya; ▲, Powell.

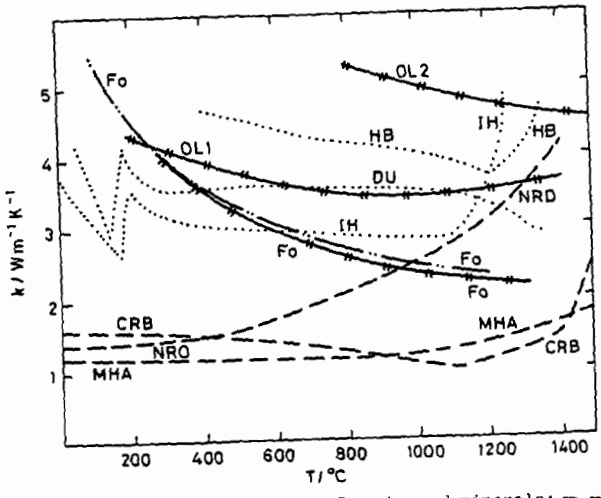

Figure 9. The thermal conductivity of rocks and minerals; — — — , Murase; ——— , Schatz; — ·—— , Kingery; ....., Kawada; the letters refer to samples.

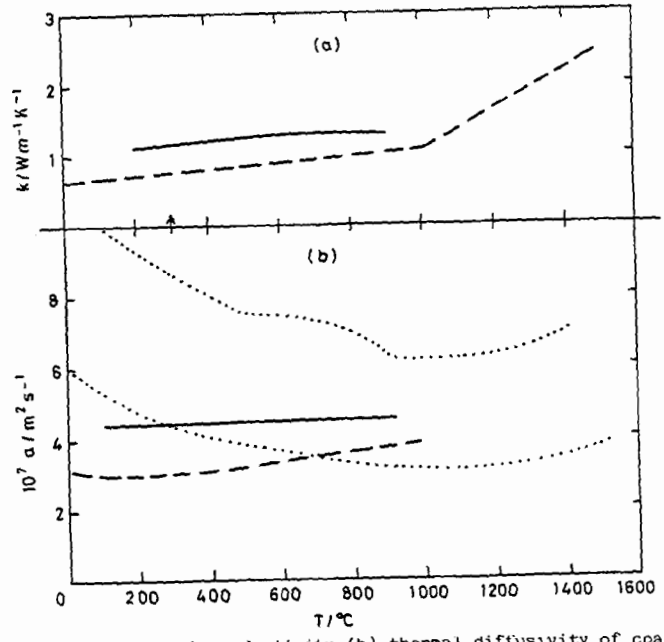

Figure 10. (a) Thermal conductivity (b) thermal diffusivity of coal slags; ———, Taylor; — — —, Vargoftik; ....., upper and lower limits of a values reported by Gibby and Bates.

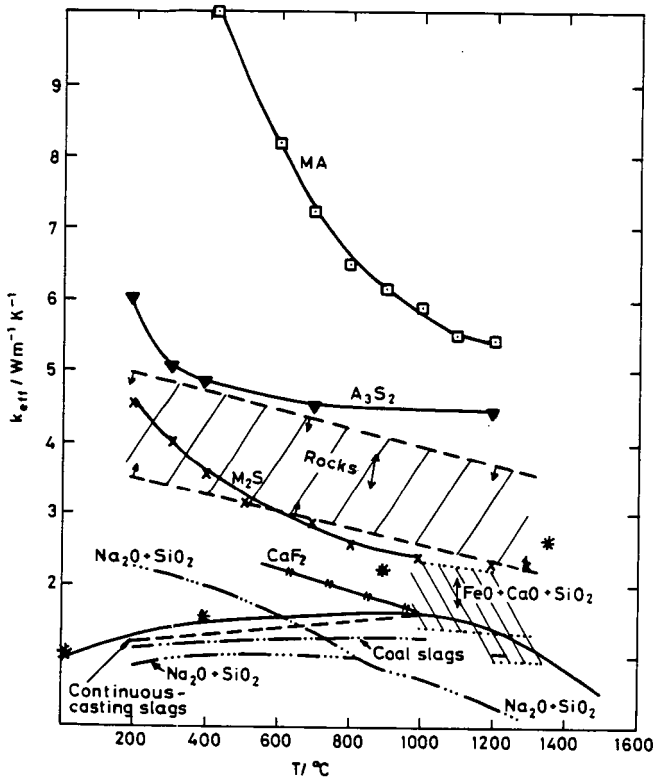

Figure 11. The thermal conductivity of various slag systems; ____, $MgO.Al_2O_3$; _____., $3Al_2O_3.2SiO_2$; _____, $2MgO.siO_2$; , upper and lower limits for data on rocks; _____, CaF_2; , data for the $FeO_x + CaO + SiO_2$ system; __ ... __, $Na_2O + SiO_2$ system; ____, $CaO + SiO_2 + Al_2O_3$ system; ___ ___ ___, continuous casting powders; = ..=, coal slags; *, k_c (glass).

SOLID-LIQUID-VAPOR INTERACTIONS IN ALKALI-RICH COAL SLAGS

L. P. Cook and J. W. Hastie

National Bureau of Standards, Washington, D.C. 20234

I. INTRODUCTION

Sodium and potassium are important constituents of the clay minerals found in most coals. As the coal is combusted these metals may be vaporized, transported and reabsorbed by slag in the cooler portions of the system, leading to the production of slags having concentrations of alkalies several times that of the primary mineral matter. Without doubt the most marked concentrations occur in slags from magnetohydrodynamic generators, where potassium is deliberately added to the combustion gases to enhance electrical conductivity of the plasma. Slags from MHD generators have K_2O concentrations approaching 20 wt%.

The corrosive effects of these high alkali slags on ceramic components of combustion systems are well known. Corrosion arises from the fact that such slags are good solvents for a wide range of materials. Furthermore, when many ceramics come into contact with high alkali slags, destructive reactions producing new solids may occur. For example, alumina, a widely used refractory, may react to produce $NaAlSiO_4$, $KAlSiO_4$ or beta alumina, depending upon the activities of silica and the alkalies. In most situations, reactions of this type would result in loss of structural integrity of the ceramic.

For these and related reasons, there is need for detailed knowledge of the physical chemistry of high alkali coal ash - derived slags. NBS has an ongoing theoretical and experimental program to systematically determine the nature of solid-liquid-vapor equilibria in high alkali coal slags. Given the wide variability of coal slag, this necessitates a close interaction between theory and experiment, if significant progress is to be made.

Experimentally, three principal methods are being utilized. Application of the high temperature quenching method, with examination of results by x-ray diffraction and electron microprobe methods, is facilitated by the fact that most silicate melts quench readily to glasses, preserving the textural and chemical relationships which prevailed under equilibrium at high temperatures. On the other hand, the relatively slow kinetics makes necessary great care in the determination of alkali vapor pressures by the Knudsen effusion/mass spectrometric method. Nonetheless the technique has been used successfully at NBS in determining vapor pressures by closely correlating effusion experiments with on-going quench experiments. Similarly, the application of the third principal experimental method, high temperature differential thermal-thermogravimetric analysis, requires a degree of caution.

There has long been interest in the development of models for the prediction of coal slag phase equilibria. While silicate phase diagrams of limited compositional range have been successfully modeled, a single model for accurate prediction of slag phase equilibra in general will require that considerably more progress be made not only in our understanding of the structural chemistry of slags but also in the availability of thermochemical data needed for such models. Progress to date is related to the realization that treatment of silicate liquids as polymerized melts may be necessary for very precise prediction of phase relationships. Also important is the discovery that alkali activities can be modeled over a wide range of compositions by treating slags as composed of mixtures of complex mineral melts such as $CaAl_2Si_2O_8$, $KAlSiO_4$, $NaAlSi_3O_8$, etc.

Thus coal slags, while not chemically ideal mixtures of the oxide components, appear to be much more ideal with respect to a choice of more complex components.

II. PHASE EQUILIBRIA IN COAL SLAGS

(A) Coal Slag As A 7-Component System

The variability of coal ash composition is directly related to variations in the proportions of mineral impurities such as SiO_2, $CaCO_3$, $CaMg(CO_3)_2$, $CaSO_4 \cdot 2H_2O$, Fe_2O_3, FeS_2, and the clay minerals which comprise a complex group of hydrated alkali aluminosilicates. Coal ashes may vary widely in their contents of iron, calcium and magnesium, but do not vary as greatly in the amount of silica and alumina they contain. In fact, of the 323 coal ash analyses reported in U.S. Bureau of Mines Bull. 567 (1), the great majority have a $SiO_2/(SiO_2+Al_2O_3)$ mole ratio between .67 and .80, with a well defined maximum near .75 (2). The bulk chemistry of the ash is related to the conditions of formation of the coal. In general lignites and subbituminous coals of the western U.S.A. are high in calcium while bituminous coals of the eastern U.S.A. contain more iron. Table 1 gives typical analyses for ashes from these coals, and includes for comparison an analysis of coal slag from a magnetohydrodynamic generator. From this table, it can be seen that, in general, coal slag must be regarded as a seven component substance, if minor constituents such as TiO_2 and P_2O_5 are ignored and if sulfur is assumed to vaporize at high temperature.

Table 1. Typical Coal Ash Analyses (wt %).

	Montana Coal[3]	Illinois Coal[3]	MHD Slag[4]
K_2O	0.4	1.4	20.2
Na_2O	0.4	1.6	0.5
CaO	11.9	8.2	3.9
MgO	3.9	0.8	1.1
Al_2O_3	21.4	16.2	12.4
Fe_2O_3	10.0	23.7	14.7
SiO_2	42.5	37.5	48.3
TiO_2	0.8	0.8	0.5
P_2O_5	0.3	0.1	-
SO_3	8.1	8.9	0.2

To account for the fact that Fe_2O_3 reduces partially to FeO with increasing temperature would require an added component. However this may be reduced again to seven if the oxygen partial pressure is included as an intensive variable along with temperature and composition. By doing this the need to specify both FeO and Fe_2O_3 in defining the bulk composition is eliminated; these are replaced by FeO_x, where x is determined by the oxygen partial pressure.

(B) Representation of Solid-Liquid-Vapor Equilibria

Ready visualization of a range of phenomena is one of the attributes making phase diagrams indispensable in understanding the chemistry of heterogeneous systems. However, although advanced multidimensional projective methods have been derived for the representation of n-component systems (5), these do not

in general lead to easily visualized diagrams. Thus for the seven component coal slag system, alternative methods must be used.

It is useful to subdivide the slag system into smaller systems. The system Al_2O_3-SiO_2 is perhaps the most fundamental system for all slags, and to this one may think of adding progressively combinations of the alkalies and CaO, MgO and FeO_x, until the desired degree of complexity is reached. Constituent systems making up the slag system are summarized in Table 2. Data are available for parts of many of these systems (6-10), but as the number of components increases, data become progressively fewer.

At NBS, experimental work is presently concentrating on the system K_2O-CaO-Al_2O_3-SiO_2. This along with K_2O-FeO_x-Al_2O_3-SiO_2 and K_2O-MgO-Al_2O_3-SiO_2, forms the basis for modeling potassium-rich slags. The approach has been to establish subsolidus equilibria (Figure 1) and then to combine these data with literature thermochemical data via solid state reactions of the type

$$A(s) + B(s) \leftrightarrow C(s) + D(s) + 2K(g) + 1/2\ O_2(g)$$

At the temperature of minimum melting, such calculations provide direct links between the phase diagram and the measurements of potassium vapor pressure which are independent of any solution model (Figure 2). This approach aides greatly in the determination of an internally consistent set of thermochemical data.

As the systems investigated become more complex (more components), other techniques may be used to reduce the number of variables, so that results can be portrayed graphically. For example, in principle phase equilibria at 1 atm in the system K_2O-CaO-FeO_x-Al_2O_3-SiO_2 could be portrayed in three dimensions graphically as a tetrahedral diagram at constant μ_{K_2O} or P_{K_2O}, T and P_{O_2}. Another way of reducing the dimensionality of the representational problem is to deal with saturation surfaces - this is actually a form of projection. For example by considering the equilibria in which Al_2O_3 participated as a phase, the need to use Al_2O_3 as a representational component would be eliminated.

(C) Role of Polymerization Theory

One of the major problems in prediction and calculation of phase equilibria is the formulation of accurate expressions for the free energy of mixing of silicate melts. Relatively few calorimetric measurements are available, and hence the importance of sound methods of estimation and prediction of mixing data to within the required degree of accuracy. Polymer theory, extended in the 1960's to include silicate melts by Masson (11) and others holds promise. It is perhaps the only general theory for silicate melts which deals quantitatively with the problem of melt structure. This has been used, with a surprising degree of success, to calculate phase equilibria in binary oxide systems (12,13). Preliminary calculations on multicomponent slags have shown that polymer theory, when treated in a quasichemical fashion, is highly flexible, and can accommodate seven component liquid immiscibility by making relatively few estimates and assumptions (Figure 3). However, attempts to fit liquidus surfaces in the system K_2O-CaO-Al_2O_3-SiO_2 have met with only partial success. Further applications and extensions of polymer theory in this quaternary system are hampered by a lack of experimental data, and an attempt is being made to rectify this situation.

Table 2. Breakdown of Lower Order Systems Comprising 7-Component Coal Slag System.

		(+CaO)	(+MgO)	(+FeO_x)	(+CaO +MgO)	(+CaO +FeO_x)	(+MgO +FeO_x)	(+CaO +MgO +FeO_x)
	Al_2O_3-SiO_2 BASE SYSTEM	CaO-Al_2O_3-SiO_2	MgO-Al_2O_3-SiO_2	FeO_x-Al_2O_3-SiO_2	CaO-MgO-Al_2O_3 -SiO_2	CaO-FeO_x-Al_2O_3 -SiO_2	MgO-FeO_x-Al_2O_3 -SiO_2	CaO-MgO-FeO_x -Al_2O_3-SiO_2
(+K_2O)	K_2O-Al_2O_3-SiO_2	K_2O-CaO-Al_2O_3 -SiO_2	K_2O-MgO-Al_2O_3 -SiO_2	K_2O-FeO_x-Al_2O_3 -SiO_2	K_2O-CaO-MgO -Al_2O_3-SiO_2	K_2O-CaO-FeO_x -Al_2O_3-SiO_2	K_2O-MgO-FeO_x -Al_2O_3-SiO_2	K_2O-CaO-MgO -FeO_x-Al_2O_3-SiO_2
(+Na_2O)	Na_2O-Al_2O_3-SiO_2	Na_2O-CaO-Al_2O_3 -SiO_2	Na_2O-MgO-Al_2O_3 -SiO_2	Na_2O-FeO_x-Al_2O_3 -SiO_2	Na_2O-CaO-MgO -Al_2O_3-SiO_2	Na_2O-CaO-FeO_x -Al_2O_3-SiO_2	Na_2O-MgO-FeO_x -Al_2O_3-SiO_2	Na_2O-CaO-MgO -FeO_x-Al_2O_3-SiO_2
(+K_2O +Na_2O)	K_2O-Na_2O-Al_2O_3 -SiO_2	K_2O-Na_2O-CaO -Al_2O_3-SiO_2	K_2O-Na_2O-MgO -Al_2O_3-SiO_2	K_2O-Na_2O-FeO_x -Al_2O_3-SiO_2	K_2O-Na_2O-CaO -MgO-Al_2O_3-SiO_2	K_2O-Na_2O-CaO -FeO_x-Al_2O_3 -SiO_2	K_2O-Na_2O-MgO -FeO_x-Al_2O_3 -SiO_2	K_2O-Na_2O-CaO-MgO -FeO_x-Al_2O_3-SiO_2 COAL SLAG SYSTEM

III. SOLUTION MODEL FOR THE PREDICTION OF ALKALI VAPOR PRESSURES

(A) Basis of the Model

The model employed for prediction of vapor pressures in multicomponent coal slags has been outlined in (14). Briefly, large negative deviations from ideal thermodynamic activity behavior are attributed to the formation of complex liquids and solids (actual components) such as K_2SiO_3, $KAlSiO_4$, etc. The free energies of formation (ΔG_f) are either known or can be estimated for these liquids and solids. By minimizing the total system free energy, one can calculate the equilibrium composition with respect to these components. Thus, for instance the mole fraction of K_2O present ($X^*_{[K_2O]}$) in equilibrium with K_2SiO_3, and other complex liquids (and solids) containing K_2O, is known. As has been shown previously for the ternary systems, the component activities can, to a good approximation, be equated to these mole fraction quantities (15). From this assumption it also follows that potassium partial pressures can be obtained from the relationship

$$P_K = \left\{2 \cdot X^*_{[K_2O]} K_p\right\}^{0.4},$$

where K_p is the stoichiometric dissociation constant for pure K_2O (liquid or solid) to K and O_2. In the following discussion the model is tested by comparing predicted P_K data determined in this manner with experimental values. Thermodynamic activities and phase compositions were also calculated using this model. The experimental K-pressure data were obtained by Knudsen effusion mass spectrometry as discussed in detail elsewhere (16).

(B) Method of Calculation

The SOLGASMIX computer program (17) used for calculation of the equilibrium composition and hence activities utilizes a data base of the type given in (14). The coefficients to the ΔG_f equation were obtained by fitting ΔG_f vs T data available in JANAF (18), Robie et al (19), Barin and Knacke (20), Rein and Chipman (21) and Kelley (22). In some cases no literature data were available and we estimated functions in the manner described earlier (16). Many of the compounds used in the calculation are mineral phases such as mullite ($Al_6Si_2O_{13}$), kaliophilite ($KAlSiO_4$), leucite ($KAlSi_2O_6$), feldspar ($KAlSi_3O_8$), and gehlenite ($Ca_2Al_2SiO_7$).

(C) Application to the K_2O-CaO-Al_2O_3-SiO_2 System

Figure 4 shows results of calculations for potassium pressures made using the model. As can be seen these agree with experimental results within limits of experimental error over a wide range of temperature. The calculations also indicate temperatures of precipitation of various solids in the quaternary system. These predictions are being checked by experiment. Other potassium pressure calculations (not shown) show similarly good agreement with experiment in the system K_2O-CaO-Al_2O_3-SiO_2.

IV. SUMMARY

An integrated experimental/theoretical approach to the problem of non-condensed (solid-liquid-vapor) phase equilibria in multicomponent coal slags has been outlined, including methods for the presentation of results. This relies upon prediction as an important tool in planning experimental work. Theory in turn benefits from experimental feedback, resulting in a continual evolution of models. Hopefully this will lead to generalized solution models capable of predicting slag phase equilibria with a high degree of accuracy.

V. REFERENCES

1. Selvig, W. A. and Gibson, F. H.: 1956, Bureau of Mines Bull. 567.
2. Cook, L. P.: 1978, Proc. 17th Symposium on Engineering Aspects of Magnetohydrodynamics, Stanford Univ., Stanford, Calif., p. C.1.2-C.1.6.
3. Petrick, M. and Shumyatsky, B. Ya., editors: "Open-Cycle Magnetohydrodynamic Electrical Power Generation" (Argonne, Illinois: Argonne National Lab.), p. 420-421.
4. Long, W.: 1978, Pers. Commun., Univ. Tenn. Space Inst.
5. Palatink, L. S. and Landau, A. I.: 1964, "Phase Equilibria in Multicomponent Systems" (New York: Holt, Rinehart and Winston).
6. Levin, E. M., Robbins, C. R. and McMurdie, H. F.: 1964, "Phase Diagrams for Ceramists" (Columbus: The American Ceramic Society).
7. Levin, E. M., Robbins, C. R. and McMurdie, H. F.: 1969, "Phase Diagrams for Ceramists, 1969 Supplement" (Columbus: The American Ceramic Society).
8. Levin, E. M., Robbins, C. R. and McMurdie, H. F.: 1975, "Phase Diagrams for Ceramists, 1975 Supplement" (Columbus: The American Ceramic Society).
9. Roth, R. S., Negas, T. and Cook, L. P.: 1981, "Phase Diagrams for Ceramists, Volume IV" (Columbus: The American Ceramic Society).
10. Roth, R. S., Negas, T. and Cook, L. P.: 1983, "Phase Diagrams for Ceramists, Volume V" (Columbus: The American Ceramic Society).
11. Masson, C. K., Smith, I. B. and Whiteway, S. G.: 1970, Canad. J. Chem., 48 1456.
12. Fraser, D. G., editor: 1976, "Thermodynamics in Geology" (Oxford, England: NATO Adv. Study Inst.).
13. Lin, P. L. and Pelton, A. D.: 1979, Metall. Trans. 10B, 667.
14. Hastie, J. W., Bonnell, D. W. and Plante, E. R.: 1983, Proc. Annual Meeting of Electrochem. Society, San Francisco, Calif.
15. Hastie, J. W., Horton, W. S., Plante, E. R., and Bonnell, D. W.: Thermodynamic Models of Alkali Vapor Transport in Silicate Systems, IUPAC Conf., Chemistry of Materials at High Temperatures, Harwell, U.K., August 1981; High Temp. High Press, in press.
16. Hastie, J. W., Plante, E. R. and Bonnell, D. W.: 1982, Alkali Vapor Transport in Coal Conversion and Combustion Systems. ACS Symp. Series, 179, p. 543-600, Gole, J. L., and Stwalley, W. C., eds. Metal Bonding and Interactions in High Temperature Systems with Emphasis on Alkali Metals (see also NBSIR 81-2279).
17. Eriksson, G.: 1975, Chemica Scripta, 8, p. 100.
18. JANAF: 1971, Joint Army, Navy, Air Force Thermochemical Tables, 2nd Ed. NSRDS-NBS 37. See also later supplements for 1971-1981.
19. Robie, R. A., Hemingway, B. S., Fisher, J. R.: 1979, Thermodynamic Properties of Minerals and Related Substances at 298.15 K and 1 Bar (10^5 Pascals) Pressure and at Higher Temperatures, Geol. Survey Bull. 1452 (Washington, D.C.: U.S. Govt. Printing Office).
20. Barin, I. and Knacke, O.: 1973, "Thermochemical Properties of Inorganic Substances" (New York: Springer Verlag).
21. Rein, R. H. and Chipman, J.: 1965, Trans. Metall. Soc. AIME, 233, p. 415.
22. Kelley, K. K.: 1962, U.S. Bur. Mines Rep. Invest., No. 5901.
23. Cook, L. P.: 1980: Proc. Seventh International Conference on MHD Electrical Power Generation, MIT, Cambridge, Mass., p. 212-219.

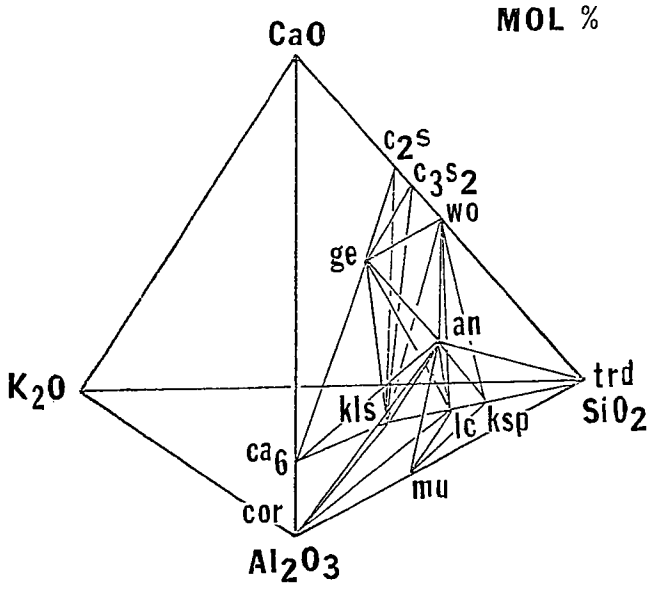

Figure 1. Experimentally determined subsolidus phase relations in the system K_2O-CaO-Al_2O_3-SiO_2.

c_2s = Ca_2SiO_4	trd = SiO_2
c_3s_2 = $Ca_3Si_2O_7$	ksp = $KAlSi_3O_8$
wo = $CaSiO_3$	lc = $KAlSi_2O_6$
ge = $Ca_2Al_2SiO_7$	kls = $KAlSiO_4$
an = $CaAl_2Si_2O_8$	mu = $3Al_2O_3 \cdot 2SiO_2$
ca_6 = $CaAl_{12}O_{19}$	cor = Al_2O_3

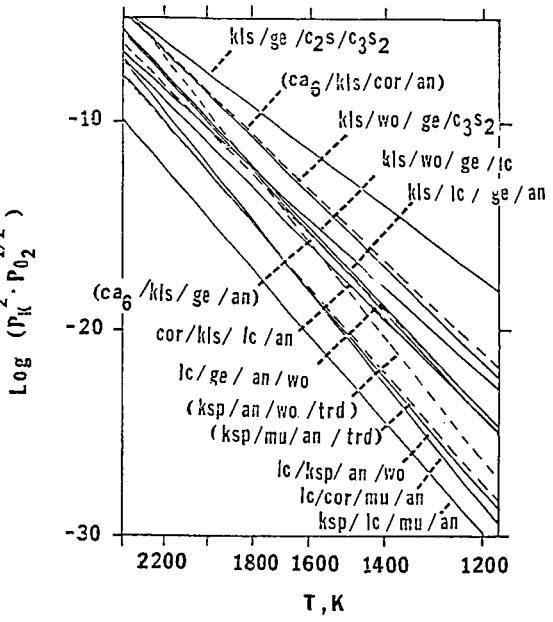

Figure 2. Calculated potassia pressures for solid assemblages in K_2O-CaO-Al_2O_3-SiO_2 (see Figure 1). Thermochemical data used were from (19). Equilibria are metastable above the minimum melting temperatures.

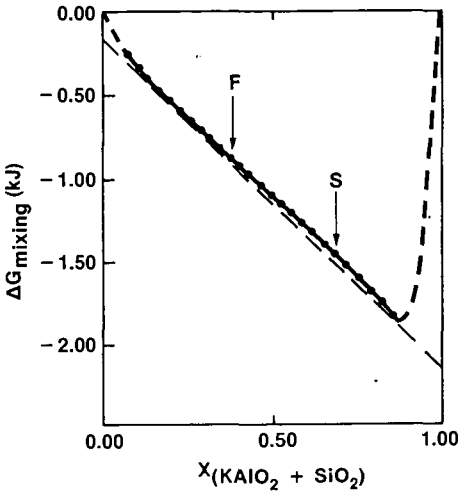

Figure 3. Calculated free energy of mixing along a compositional vector in the system K_2O-CaO-MgO-FeO_x-Al_2O_3-SiO_2 passing through experimentally determined compositions of immiscible melts (F and S). Calculations were made using the quasi-chemical melt polymerization theory (23). The compositions of predicted and observed immiscible melts can be made to agree reasonably well by adjustments in polymerization equilibrium constants and in the ratio $Fe^{+3}/(Fe^{+3} + Fe^{+2})$.

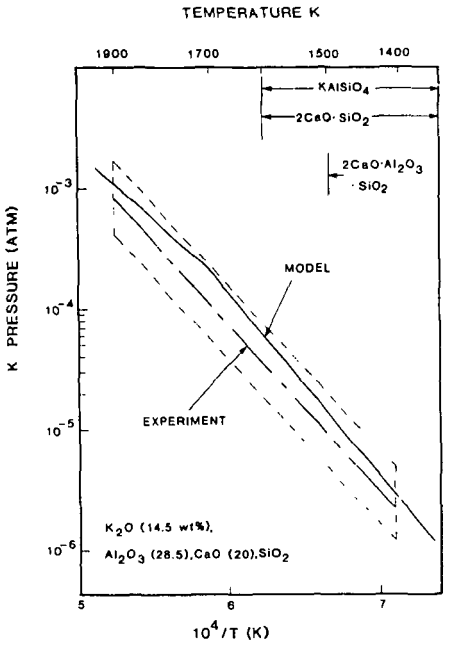

Figure 4. Comparison of ideal mixing of complex components solution model (solid curve) and experimental (broken curve) K-pressure data as a function of reciprocal temperature, for a composition in the K_2O-CaO-Al_2O_3-SiO_2 system. Compounds listed are solid precipitates formed over the temperature interval indicated.

OVERVIEW OF COAL ASH DEPOSITION IN BOILERS

R. W. Borio and A. A. Levasseur

COMBUSTION ENGINEERING, INC.
1000 Prospect Hill Road, Windsor, CT 06095

INTRODUCTION

The management of coal ash in utility boilers continues to be one of the most important fuel property considerations in the design and operation of commercial boilers. The behavior of mineral matter in coal can significantly influence furnace sizing, heat transfer surface placement, and convection pass tube spacing. Ironically, many of the more reactive, low rank U. S. coals must have larger furnaces than the less reactive higher rank coals. This is strictly a requirement based on the mineral matter behavior; Figure 1 illustrates this point. Given the same mineral matter behavior the more reactive, lower rank coals would require less residence time and therefore smaller furnace volumes than the less reactive, higher rank coals.

Although pulverized coal has been fired for more than 50 years and much is known about combustion behavior there are still a number of boilers experiencing operational problems from coal ash effects. Ash-related problems are one of the primary causes of unscheduled outages, unit derating and unavailability. Because of variability in a given coal seam and since many boiler operators may experience changes in their coal supply during the life of a boiler, operational problems caused by changes in coal ash properties can significantly affect boiler performance. Not only must the initial boiler design be correctly determined based on the specification coal but reliable judgements must be made regarding the suitability of other candidate coals and their effect on operation during the lifetime of the boiler.

The increased emphasis on coal usage in this country and, indeed, the significant effort underway to consider coal water mixtures as possible oil substitutes in oil-designed boilers underscores the need to improve the prediction of mineral matter behavior in a boiler environment.

Coal is a very heterogeneous, complex material which produces heterogeneous, complex products during combustion. Since, during pulverized coal combustion, coal particles of various organic and mineral matter compositions can behave in completely different manners, prediction based upon the overall or average composition may be misleading. Like many of the currently-used ASTM coal analyses, the method for determining ash fusibility temperatures was developed when stoker firing was a predominant coal firing technique; the methodologies and conditions employed during many of the ASTM tests reflect this. It is not surprising that the usefulness of some ASTM test results may be limited when used for a pulverized coal firing application. In recent years researchers have developed methodologies for characterizing coal ash behavior that better reflect the fundamental mechanisms controlling behavior and more closely simulate the conditions that exist in a pulverized coal fired boiler.

Clearly there is a need for improved mineral matter behavior predictive techniques. This paper will provide a statement of the ash deposition problem in pulverized coal fired boilers, it will present an assessment of the older, traditional methods for predicting mineral matter behavior and it will address some of the newer techniques that have been suggested as better ways of characterizing coal ash behavior. Additionally some areas of uncertainty will be identified as requiring the development of better predictive techniques.

STATEMENT OF THE PROBLEM

The presence of ash deposits and flyash can create the following problems in a boiler:

1. Reduced heat transfer
2. Impedance of gas flow
3. Physical damage to pressure parts
4. Corrosion of pressure parts
5. Erosion of pressure parts

These problems can result in reduced generating capacity, unscheduled outages, reduced availability, and costly modifications.

Ash which deposits on boiler walls in the radiant section of a furnace is generally referred to as slagging. Ash deposition on convection tube sections downstream of the furnace radiant zone is typically referred to as fouling. Ash slagging and fouling can result in problems listed in items 1 through 4; item 5, erosion, is the result of impingement of abrasive ash on pressure parts. Often coal ash deposit effects are inter-related. For example, slagging will restrict waterwall heat absorption changing the temperature distribution in the boiler which in turn influences the nature and quantity of ash deposition in downstream convective sections. Ash deposits accumulated on convection tubes can reduce the cross-sectional flow area increasing fan requirements and also creating higher local gas velocities which accelerates flyash erosion. In situ deposit reactions can produce liquid phase components which are instrumental in tube corrosion.

One of the most common manifestations of a deposition problem is reduced heat transfer in the radiant zone of a furnace. Decreased heat transfer due to a reduction in surface absorptivity is a result of the combination of radiative properties of the deposit (emissivity/absorptivity) and thermal resistance (conductivity) of a deposit. Thermal resistance (thermal conductivity and deposit overall thickness) is usually more significant because of its effect on absorbing surface temperature.

Previous work has indicated that the physical state of the deposit can have a significant effect on the radiative properties, specifically molten deposits show higher emissivities/absorptivities than sintered or powdery deposits (Ref. 1). Although thin, molten deposits are less troublesome from a heat transfer aspect than thick, sintered deposits, molten deposits are usually more difficult to remove and cause frozen deposits to collect in the lower reaches of the furnace; physical removal then becomes a problem for the wall blowers.

Impedance to gas flow is the result of heavy fouling on tubes in the convective section. Problems of this type are most likely to occur with coals having high sodium contents, usually found in low rank coal deposits in Western U.S. seams. Hard, bonded deposits can occur which are resistant to removal by the retract soot-blowers.

Physical damage to pressure parts can occur if large deposits have accumulated in the upper furnace and proceed to become dislodged or blown off and drop onto the slopes of the lower furnace. Such deposits are usually characterized by their relatively high bonding strengths and their heavily sintered structure.

Fireside corrosion can occur on both waterwall and superheater tube surfaces. Normal sulfates and pyrosulfates are frequently the cause of waterwall corrosion, although reducing conditions can also cause depletion of protective oxide coatings on tube surfaces. On higher temperature metal surfaces, (superheaters/reheaters) alkali-iron-trisulfates are often the cause of corrosion. Chlorine can also be a contributing factor toward superheater metal corrosion. While exact mechanisms can be argued there have been examples of both liquid phase and gas phase corrosion when chlorides have been present (Ref. 2).

Erosion of convective pass tubes, while not a function of deposits, is caused by the abrasive components in flyash. Flyash size and shape, ash particle composition and concentration, and local gas velocities play important roles concerning erosion phenomenon. Recent work has shown that quartz particles above a certain particle size are very influential in the erosion process and that furnace temperature history plays an important role in determining erosive characteristics of the particles (Ref. 3 & 4).

FUNDAMENTAL CONSIDERATIONS IN ASH DEPOSITION

The coal ash deposition process is extremely complex and involves numerous aspects of coal combustion and mineral transformation/reaction. The following all play a role in the formation of ash and the depositon process.

Coal Organic Properties
Coal Mineral Matter Properties
Combustion Kinetics
Mineral Transformation and Decomposition
Fluid Dynamics
Ash Transport Phenomena
Vaporization and Condensation of Ash Species
Deposit Chemistry - Specie Migration and Reaction
Heat Transfer To and From the Deposit

Despite considerable research in these areas, there are many gaps in our fundamental understanding of the mechanisms responsible for mineral matter behavior. Although substantial knowledge exists concerning the deposition process, the complexity of the subject does not allow detailed discussion here. However, the importance of furnace operating conditions on the combined results of each of the above areas must be stressed. For a given coal composition, furnace temperatures and residence times generally dictate the physical and chemical transformations which occur. The ash formation process is primarily dependent on the time/temperature history of the coal particle. The resultant physical properties of a given ash particle generally determine whether it will adhere to heat transfer surfaces. Local stoichiometries can also influence the transformation process and thereby the physical characteristics of ash particles; iron-bearing particles are a prime example of this.

Aerodynamics can play a role in the ash deposition process in all furnaces regardless of the type of firing; recent interest in microfine grinding of coal is testimony to this fact. It has been postulated that smaller ash particles will follow gas streamlines and be less likely to strike heat transfer surfaces. This is a logical hypothesis for those ash particles that cause deposition due to an impact mechanism. In addition to particle size, particle density and shape also affect aerodynamic behavior. Molten, spherical particles will be less likely to follow gas streamlines than angular or irregular particles of the same mass due to the difference in drag forces.

Most coal ash will result in deposits of increasing severity with increasing gas temperature. This is not a linear relationship, as illustrated in Figure 2, but rather shows a progressively more severe ash deposit condition with increasing gas temperature (Ref. 5). Boilers are normally designed so that cleanable, sintered deposits will be formed. This is a reasonable compromise between a very large, economically uncompetitive boiler that may produce very dry, dusty deposits and a very small, highly loaded boiler that would produce molten, running ash deposits.

The key governing factor, then, is determining how small a furnace can be, for a given MW output, and still result in deposits that are cleanable with conventional sootblowing equipment.

Because of the complexity of the ash formation and ash deposition process, it seems logical to deal first with those key coal constituents most responsible for ash deposition. The iron and sodium contents of an ash have typically been considered key constituents. Techniques have been developed to determine how these key constituents are contained in the coal, i.e., the particular mineral forms that are present or the grain size of the constituent in question. Obviously the remainder of the mineral matter has an effect, but depending on the concentration and form in which iron and/or sodium constituents are present, the remaining mineral matter often has second order effects.

As previously discussed, ash formation and the resulting ash size distribution is extremely complex and is dependent on several factors including initial coal size, coal burning characteristics, mineral content, mineral grain size, volatile ash species, melting behavior of the mineral matter, and temperature history of the particle. Generally, coal containing lower melting mineral matter has a greater potential for ash agglomeration as the particle burns and yields fewer ash particles per coal particle which results in coarser ash particles than those of coal with higher melting ash. Obviously things like ash quantity, and mineral grain sizes could influence this hypothesis. The way a coal particle burns may also influence the number of ash particles generated, i.e., a shrinking sphere burning mode may produce a different result from a constant diameter, decreasing density mode of burning; swelling coals may behave differently than non-swelling coals.

In reflecting on the above discussion, it becomes apparent that one cannot completely divorce the predictive techniques employed, from the particular coal burning application. Pulverized coal firing will require a sensitivity to different conditions than stoker firing, or a slagging combustor. Failure to address the specific conditions inherent in each type of firing system will lead to lower resolution in one's predictive abilities than desired.

ASSESSMENT OF TRADITIONAL PREDICTIVE METHODS

ASTM measurements such as ash fusibility (D1857) have formed the basis for traditional ash behavior predictive techniques. These bench-scale tests provide relative information on a fuel; this is used in a comparative fashion with similar data on fuels of known behavior. Unfortunately, the commonly used tests do not always provide sufficient information to permit accurate comparison.

The fusibility temperature measurement technique attempts to recognize the fact that mineral matter is made up of a mixture of compounds each having their own melting point. As a cone of ash is heated some of the compounds melt before others and a mixture of melted and unmelted material results. The structural integrity or deformation of the traditional ash cone changes with increasing temperature as more

of the minerals melt. However, more recent results indicate that significant melting/sintering can occur before initial deformation is observed (Ref. 6). The fact that the time/temperature history of laboratory ash is quite different from conditions experienced in the boiler can result in difference in melting behavior. In addition, the ash used in this technique may not represent the composition of ash deposits that actually stick to the tube surfaces. Often there is a major discrepancy between the composition of as-fired ash and that which is found as deposits (See Table I). This is a major criticism of the ash fusibility temperatures. The discrepancies between fusibility temperature predictions and actual slagging performance is usually greater on ashes that may look reasonably good based on fusibility temperature results. One can usually assume, with reasonable confidence, that the melting temperature of the waterwall deposits will be no higher than ASTM fusibility temperatures; but deposit melting temperatures can be and are often lower than ASTM melting temperatures. This is because selective deposition of lower melting constituents can and does occur; hence there is an enrichment of lower melting material in the deposit.

Ash viscosity measurements suffer similar criticism to the fusibility measurements. These tests are conducted on laboratory ash and on a composite ash sample. Viscosity measurements are less subjective and more definitive than fluid temperature determination for the assessment of ash flow characteristics. However, these measurements reflect the properties of a totally dissolved solution of ash constituents and may not be representative of slag deposit properties in pulverized coal-fired boilers. During pulverized coal firing, a severe problem may already exist before slag deposits reach the fluid/running state. Generally, only a small quantity of liquid phase material exists in deposits and it is the particle-to-particle surface bonding which is most important.

Much use is made of the ash composition which is normally a compilation of the major elements in coal ash expressed as the oxide form. From this compilation of elements, expressed as oxides, judgements are often made based on the quantity of certain key constitutents like iron and sodium. Base/acid ratios are computed and used as indicators of ash behavior; normally lower melting ashes fall in the 0.4 to 0.6 range. It has been shown that base/acid ratios generally correlate with ash softening temperatures, so although base/acid ratios have helped explain why ash softening temperatures varied, it has not improved predictive capabilities in the authors' opinion. Other ratios such as Fe/Ca and Si/Al have been used as indicators of ash deposit behavior. Ratios like these have helped to explain deposit characteristics, but their use as a prime predictive tool is questionable especially since these ratios do not take into account selective deposition nor do they consider the total quantities of the constituents present. An Fe/Ca ratio of 2 could result from 6/3 or 30/15; the latter numbers would generally indicate a far worse situation than the former, but ratios don't show this.

Many slagging and fouling indices are based upon certain ash constituent ratios and corrected using such factors as geographical area, sulfur content, sodium content, etc. One commonly used slagging index uses Base/Acid ratio and sulfur content. Factoring in sulfur content is likely to improve the sensitivity of this index to the influence of pyrite on slagging. (As previously discussed, iron-rich minerals often play an important role in slagging.) However, the use of such "correction" factors is often a crude substitute for more detailed knowledge of the fundamental fuel properties. Another example of this is the use of chlorine content in a coal as a fouling index. This can be true if the chlorine is present as NaCl thereby indicating the concentration of sodium which is in an active form and that will, in fact, cause the fouling. Chlorine present in other forms may or may not adversely affect fouling.

Sintering strength tests have been used as an indication of fouling potential. Assuming that correct ash compositions have been represented (which is less of a problem in the convection section than in the radiant section) worthwhile information may be obtained relative to a time/temperature vs. bonding strength relationship. In order for sintering tests to accurately predict actual behavior it is necessary that tests be conducted with ash produced under representative furnace conditions (time-temperature history). Fouling behavior is often greatly influenced by sodium reactions. Sodium which vaporizes in the furnace can condense in downstream convection sections thereby concentrating on flyash surfaces. Particle surface reactions are primarily responsible for convection deposit bonding.

In summary, traditional methods for prediction ash deposit characteristics are heavily based upon ash chemistry. These convectional analyses do not provide definitive information concerning the mineral forms present in the coals and the distribution of inorganic species within the coal matrix. Such information can be extremely important in extrapolating previous experience, since the nature in which the inorganic constituents are contained in the coal can be the determining factor in their behavior during the ash deposition process.

ASSESSMENT OF NEW PREDICTIVE TECHNIQUES

Generally speaking the newer bench scale predictive techniques are far more sensitive to the conditions that exist in commercial furnaces than the older predictive methods. Selective deposition, for example, has been recognized as a phenomenon which cannot be ignored. More attention is being paid to fundamentals of the ash formation and deposition processes. New tools, such as Scanning Electron Microscopy (SEM), are being considered as ways to improve predictive capabilities. Other, more specialized bench scale apparatuses are being developed to simulate important aspects of commercial conditions and provide quantitative information on parameters that influence bonding strength.

Recent work has shown that pulverized coal, if separated by gravity fractionation, can yield important information relative to slagging potential due to the iron content. (Ref. 6, 7). Results of this work have shown that the percentage of iron in the heavy fractions correlates very well to the slagging behavior in commercial boilers. (See Figure 3). This technique appears to identify the proportion of relatively pure pyrites particles that are generated in the pulverized coal feed and that are capable of melting at relatively low temperatures and that would account for enrichment of iron in lower furnace waterwall deposits.

A method for measuring active alkalies has been developed as a means for improved prediction of fouling potential (Ref. 8). Previous wisdom held that fouling potential was directly related to the total sodium content. Much of this early work was done on low rank coals in which case it was not uncommon for all of the alkalies to be present as an active sodium form (Ref. 9). However, there were many occasions where the fouling potential was not adequately predicted by the total sodium content. (Table II provides some examples of anomalous fouling behavior.) The mechanism postulated for sodium-related fouling was one of a vaporization/condensation mechanism. Simple forms of sodium compounds resulted in the vaporization of sodium in the radiant zone of the furnace where peak temperatures are generated. Subsequent condensation of the sodium on the relatively cool tube surfaces effected a process for deposition of sodium. Sodium is a known, effective fluxing agent that can create hard, bonded deposits. The referenced method relied on the use of weak acid to preferentially leach out sodium from simple compounds like NaCl and/or organically-bound alkali as would be present in many of the lower rank coals. This method gives results that correlate well with field performance on coals having significant sodium contents (See Table II).

The use of new analytical techniques promises to give results that allow mineral matter to be identified according to composition, mineral form, distribution within the coal matrix, and grain size.

Techniques such as computer-controlled scanning electron microscopy (CCSCM) transmission electron microscopy (STEM), X-ray diffracton can be used to characterize these properties on individual particle by particle basis. New spectroscopies such as extended X-ray absorption of fine structure spectroscopy (EXAFS), and electron energy loss spectroscope, (EELS) are capable of determining electronic bonding structure and local atomic environment for organically associated inorganics like calcium, sodium and sulfur. Other new techniques such as Fourier transform infrared spectroscopy (FTIR), electron microprobe, electron spectroscopy for chemical analysis (ESCA), etc. all provide methods of improving present capabilities. By development and application of these techniques a much better fundamental assessment of coal mineral matter behavior is possible. The authors believe these results, coupled with those of other existing methods, can make a significant improvement to predictive capabilities.

AREAS OF UNCERTAINTY

Prediction of ash deposit characteristics based solely on bench-scale fuel properties always requires substantial judgement and allows only a certain level of confidence. As discussed, the ash deposition process is so complex that detailed modelling of commercial systems based on fundamental data is presently unrealistic. However, current techniques can provide relative data which in most cases is sufficient to make accurate assessment of slagging and fouling potentials relative to other fuels.

There remains many areas of uncertainty where experienced judgements must fill the gap between good laboratory results/predictions and boiler design decisions. One of these areas concerns the extent of deposit coverage in a boiler. Though the fuels researcher may adequately characterize a given coal ash in terms of its potential deposit effects, he is often at a loss to adequately describe the extent of coverage of deposits in the boiler. It is necessary to accurately describe furnace conditions in order to assess resulting deposits in particular boiler regions. Though some good work is underway in this area, the question of bonding strength and cleanability remains a problem as far as its prediction from bench scale tests. Though some good correlations have been developed between iron content of heavy gravity fractions and slagging, there does not exist a bench scale technique that can simulate what the ash deposit composition shall be when burned in a commercial boiler.

It is possible to increase the level of confidence for prediction of deposit effects by conducting pilot-scale combustion studies in test rigs which more closely simulate the conditions present in commercial boilers. Combustion testing allows evaluation of the ash formation and deposition process and permits detailed characterization of deposits generated. Results can allow determination of deposit characteristics as a function of fundamental boiler design parameters (such as gas temperature, velocity, etc.). Combustion test rigs also serve as valuable tools for assessment of fuels with very unusual properties and can significantly reduce uncertainties in extrapolation of their behavior from past experience.

Whenever test results are assessed and used to establish boiler design parameters, the representativeness of the test sample must be carefully considered. The degree of variability in the coal deposit and its impact on the day-to-day fuel properties

are very important factors which must be evaluated. Judgements are also required on long term coal supply properties.

In summary, it can be stated that the ash formation and deposition process is not fully understood. Traditional ASTM analyses do not always provide information that can be used to make predictive judgements at the confidence levels desired. Newer techniques have been developed and are being developed that are more sensitive to the conditions that exist in the boiler environment, and that recognize the heterogeneity of the inorganic constituents in the coal matrix. There appears to be a recognition that no one test can adequately describe coal ash behavior; a combination of tests, each designed to focus on a particular aspect of ash behavior seems to be a logical approach. Based on the results from many of these newer tests, on coals that are presently being burned in existing units, the authors feel certain that significant improvements have been made in predicting ash behavior. Finally the authors suggest that attention be given, by cognizant people, to the idea of standardizing some of the newer predictive techniques and incorporating them as supplements to existing ASTM tests.

REFERENCES

1. G. J. Goetz, N. Y. Nsakala, and R.W. Borio, "Development of Method for Determining Emissivities and Absorptivities of Coal Ash Deposits," paper presented at the 1978 Winter Annual ASME Meeting, Dec. 1978, TIS-5890.

2. R. W. Borio, et.al., "The Control of High Temperature Fireside Corrosion in Utility Coal-Fired Boilers," ORC R&D Report No. 41 (1969).

3. F. Raask, "Flame Imprinted Characteristics of Ash Relevant to Boiler Slagging Corrosion and Erosion," presented at the 1981 Joint Power Generation Conference, ASME Paper No. 81-JPGC-Fu-1.

4. W. P. Bauver, J. D. Bianca, J. D. Fishburn, and J. G. McGowan, "Characterization of Erosion of Heat Transfer Tubes in Coal-Fired Power Plants," paper to be presented at 1984 Joint Power Generation Conference, Toronto, Canada, September 1984.

5. R. W. Borio, G. J. Goetz, and A. A. Levasseur, "Slagging and Fouling Properties of Coal Ash Deposits as Determined in a Laboratory Test Facility," paper presented at the ASME Winter Annual Meeting, December 1977, Combustion Engineering publication TIS-5155.

6. J. P.Huffman and F.E. Higgins, "Investigations of Partial Ash Melting by Phase Analysis of Quenched Samples," presented at 1981 Engineering Foundation Conference-Fouling and Slagging Resulting From Impurities in Combustion Gases, July 1981, Henniker, NH.

7. R. W. Borio, R. R. Narciso, Jr., "The Use of Gravity Fractionation Techniques for Assessing Slagging and Fouling Potential of Coal Ash," paper presented at the ASME Winter Annual Meeting, December 10-15, 1978, San Francisco, CA; available as Combustion Engineering publications TIS-5823.

8. R. W. Bryers, "The Physical and Chemical Characteristics of Pyrites and Their Influence on Fireside Problems in Steam Generators, "ASME Paper No. 75-WA/CD-2, 1976.

9. G. L. Hale, A. A. Levasseur, A. L. Tyler and R. P.Hensel, "The Alkali Metals in Coal: A Study of Their Nature and Their Impact on Ash Fouling," paper presented at Coal Technology '80, November 1980, TIS-6645.

10. G. H. Gronhovd, W. Beckering, and P. H. Tlufte, "Study of Factors Affecting Ash Deposition from Lignite and Other Coals," an ASME publication presented at the ASME Winter Annual Meeting, November 16-20, 1969, Los Angeles, CA.

FIGURE 1

EFFECT OF COAL PROPERTIES ON FURNACE SIZE

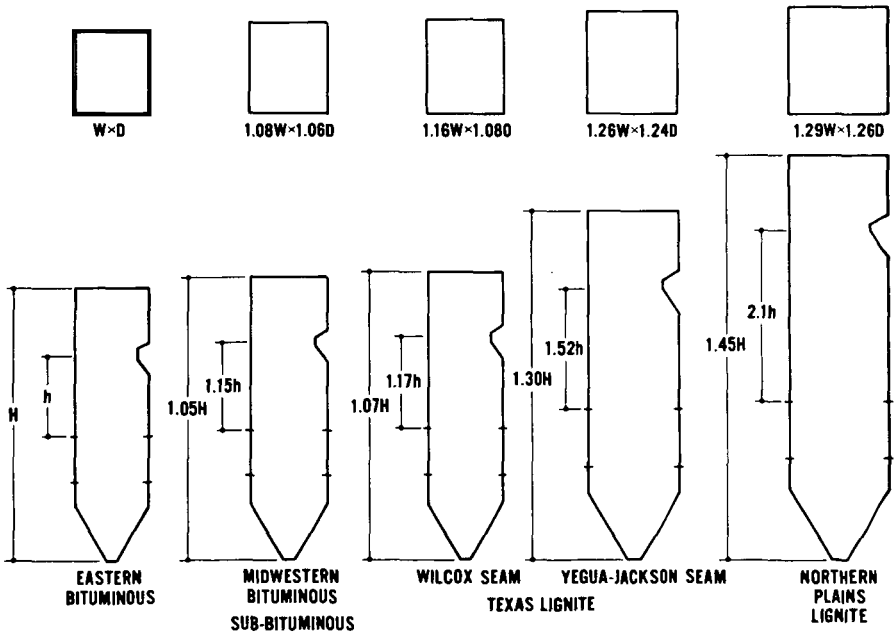

FIGURE 2

SUPERHEATER DEPOSIT BUILDUP vs FLUE GAS TEMPERATURE

DEPOSIT COLLECTED IN 8 HOUR PERIOD
DEPOSIT WEIGHT NORMALIZED: (DEPOSIT WT./(ASH INPUT
× SURFACE AREA OF COLLECTION)

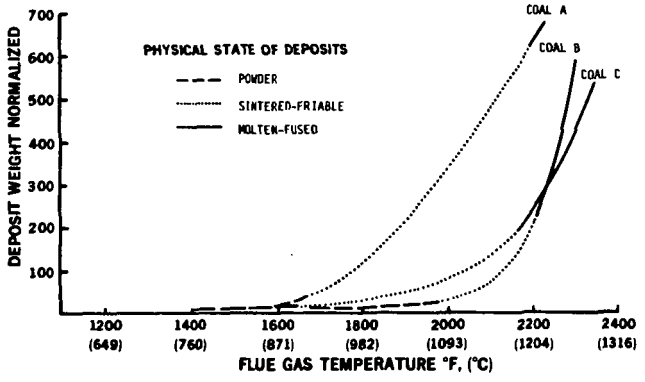

FIGURE 3

EFFECT OF SEGREGATED IRON ON COAL ASH SLAGGING
SLAGGING POTENTIAL
VERSUS
PERCENT IRON IN 2.9 GRAVITY FRACTION

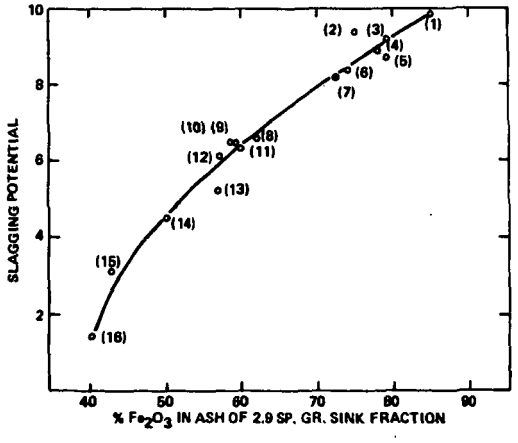

TABLE I

ENRICHMENT OF IRON IN BOILER WALL DEPOSITS
COMPARISON OF COMPOSITION OF ASH
DEPOSITS AND AS-FIRED COAL ASHES

UNIT	1		2		3	
SAMPLE	AS-FIRED COAL ASH	WATERWALL DEPOSIT	AS-FIRED COAL ASH	WATERWALL DEPOSIT	AS-FIRED COAL ASH	WATERWALL DEPOSIT
Ash Composition						
SiO_2	47.0	33.3	50.2	55.1	49.7	41.8
Al_2O_3	26.7	18.0	16.9	14.6	16.5	15.8
Fe_2O_3	14.6	43.5	5.9	18.3	12.0	28.5
CaO	2.2	1.2	12.8	7.2	6.5	9.0
MgO	0.7	0.5	3.5	2.0	0.9	0.9
Na_2O	0.4	0.2	0.6	0.5	1.1	0.6
K_2O	2.3	1.6	0.8	0.6	1.5	0.9
TiO_2	1.3	0.8	0.9	0.8	1.1	0.7
SO_3	1.1	0.5	12.0	0.1	2.0	0.2

TABLE 2 ANALYTICAL DATA ON U.S. COALS

Rank Region	Lignite N. Dakota	Sub B Montana	Lignite Texas (Yegua)	Lignite Texas (Wilcox)	hvBb Utah	hvAb Penn	Lignite Texas (Wilcox)
(Dry Basis)							
Volatile	44.4	42.2	39.6	41.0	41.5	32.5	38.1
Fixed C	46.0	52.0	26.9	39.5	48.3	54.0	33.0
Ash	9.6	5.6	33.5	19.5	10.2	13.5	28.9
HHV (Btu/lb) (Dry Basis)	10640	12130	7750	9710	12870	13200	8420
Ash Fusibility							
I.D. (°F)	2130	1980	1940	2150	2190	2370	2210
S.T.	2180	2020	2200	2250	2270	2510	2300
H.T.	2190	2060	2430	2340	2390	2560	2420
F.T.	2200	2170	2610	2530	2620	2660	2620
Ash Composition							
SiO_2 (%)	20.0	33.9	62.1	52.3	52.5	51.1	57.9
Al_2O_3	9.1	11.4	15.1	17.4	18.9	30.7	21.8
Fe_2O_3	10.3	10.8	3.5	5.3	1.1	10.0	3.9
CaO	22.4	21.0	6.2	9.4	13.2	1.6	7.1
MgO	6.4	2.7	0.7	3.2	1.3	0.9	2.1
Na_2O	5.0	5.8	3.6	0.9	3.8	0.4	0.9
K_2O	0.5	1.6	2.1	1.2	0.9	1.7	0.8
TiO	0.4	0.7	0.9	1.2	1.2	2.0	1.1
SO_3	21.9	12.0	6.1	9.6	6.2	1.4	4.4
Total alkali, %, ash basis							
Na_2O	5.0	5.8	3.6	0.9	3.8	0.4	0.7
K_2O	0.5	1.6	1.9	1.2	0.9	1.7	0.8
Soluble Alkali, %, ash basis							
Na_2O	5.58	6.45	3.88	0.71	1.49	0.15	0.16
K_2O	—	—	0.44	0.04	0.08	—	0.05
Relative Soluble Alkali, %							
Na_2O	112%	111%	108%	79%	39%	38%	23%
K_2O	—	—	—	3%	9%	—	6%
Fouling Potential	**Severe**	**High**	**High**	**Moderate**	**Moderate**	**Low**	**Low**